AGU PUBLICATIONS

Geochemistry, Geophysics, Geosystems

RESEARCH ARTICLE
10.1002/2016GC006641

Fitful and protracted magma assembly leading to a giant eruption, Youngest Toba Tuff, Indonesia

Mary R. Reid [1] **and Jorge A. Vazquez** [2]

[1]School of Earth Sciences and Environmental Sustainability, Northern Arizona University, Flagstaff, Arizona, USA, [2]U.S. Geological Survey, Menlo Park, California, USA

Key Points:
- Zircon nucleation and growth in the Youngest Toba Tuff magma reflect diverse conditions and protracted time intervals of >100 to >500 ka
- Zircon growth was intermittent as a result of spatiotemporal variations in magma reservoir composition
- Episodic magma recharge accounted for magma reservoir longevity and contributed to compositional zoning

Supporting Information:
- Supporting Information S1
- Table S1
- Table S2
- Table S3
- Table S4
- Table S5
- Table S6
- Table S7

Correspondence to:
M. R. Reid,
mary.reid@nau.edu; 928-523-7200

Citation:
Reid, M. R., and J. A. Vazquez (2017), Fitful and protracted magma assembly leading to a giant eruption, Youngest Toba Tuff, Indonesia, *Geochem. Geophys. Geosyst.*, *18*, 156–177, doi:10.1002/2016GC006641.

Received 9 SEP 2016
Accepted 5 DEC 2016
Accepted article online 20 DEC 2016
Published online 22 JAN 2017

Abstract The paroxysmal eruption of the 74 ka Youngest Toba Tuff (YTT) of northern Sumatra produced an extraordinary 2800 km^3 of nonwelded to densely welded ignimbrite and coignimbrite ashfall. We report insights into the duration of YTT magma assembly obtained from ion microprobe U-Th and U-Pb dates, including continuous age spectra over >50% of final zircon growth, for pumices and a welded tuff spanning the compositional range of the YTT. A relatively large subpopulation of zircon crystals nucleated before the penultimate caldera-related eruption at 501 ka, but most zircons yielded interior dates 100–300 ka thereafter. Zircon nucleation and growth was likely episodic and from diverse conditions over protracted time intervals of >100 to >500 ka. Final zircon growth is evident as thin rim plateaus that are in Th/U chemical equilibrium with hosts, and that give crystallization ages within tens of ka of eruption. The longevity and chemical characteristics of the YTT zircons, as well as evidence for intermittent zircon isolation and remobilization associated with magma recharge, is especially favored at the cool and wet eutectoid conditions that characterize at least half of the YTT, wherein heat fluxes could dissolve major phases but have only a minor effect on larger zircon crystals. Repeated magma recharge may have contributed to the development of compositional zoning in the YTT but, considered together with limited allanite, quartz, and other mineral dating and geospeedometry, regular perturbations to the magma reservoir over >400 ka did not lead to eruption until 74 ka ago.

1. Aspects of the Shallow Magma Reservoir Responsible for the Youngest Toba Tuff

The 74 ka Youngest Toba Tuff (YTT) is the product of a caldera-forming "supereruption" in northern Sumatra, and records "the largest volcanic eruption experienced by the modern human race" [*Chesner*, 2012]. A monumental 2800 km^3 of rhyolite was likely vented from a melt-rich subvolcanic reservoir located at a depth of ~3–4 km [*Chesner and Luhr*, 2010]. Judging by the 30 × 100 km footprint of Toba Caldera (Figure 1) and the sill-like magmatic complex imaged seismically below it, the associated intrusive complex is batholithic in scale [*Jaxybulatov et al.*, 2014; *Karlstrom et al.*, 2012]. The reservoir could have been sustained as an incrementally fed shallow reservoir [*Annen*, 2009; *Gelman et al.*, 2013], assuming development since the penultimate eruption at 501 ka [*Chesner et al.*, 1991] and an extrusive:intrusive ratio ≥1:3 [*White et al.*, 2006], and therefore an average magma output of at least 2.6 × 10^{-3} km^3/yr. Generation of suchzones of shallow magma accumulation and the persistence of eruptible domains within them are subject to considerable debate (e.g., *Paterson and Ducea* [2015], *Lundstrom and Glazner* [2016], and associated edited volumes). Whatever their origins, eruptions of the magnitude of the YTT present a serious threat for society [*Self*, 2006]: atmospheric loading by aerosols and ash might have accelerated cooling of Earth's climate and resulted in near extinction of humans [*Petraglia et al.*, 2012, and references therein].

An extraordinary feature of the YTT, beyond its gigantic size, is the extensive differentiation that must be responsible for its dominantly high-silica composition [*Chesner and Luhr*, 2010]. Associated with this are subordinate crystal-rich domains (30–40%) that could represent hotter and less differentiated melts, or domains that accumulated crystals in response to two-phase flow [*Chesner*, 1998; *Chesner and Luhr*, 2010]. YTT glasses are characterized by a range of compositions consistent with variable crystal-melt fractionation [*Westgate et al.*, 2013; *Gatti et al.*, 2014]. If longstanding, chemical and mineralogical stratification could account for stability of the magmatic reservoir in the aftermath of a 501 ka caldera-forming eruption. Mineral

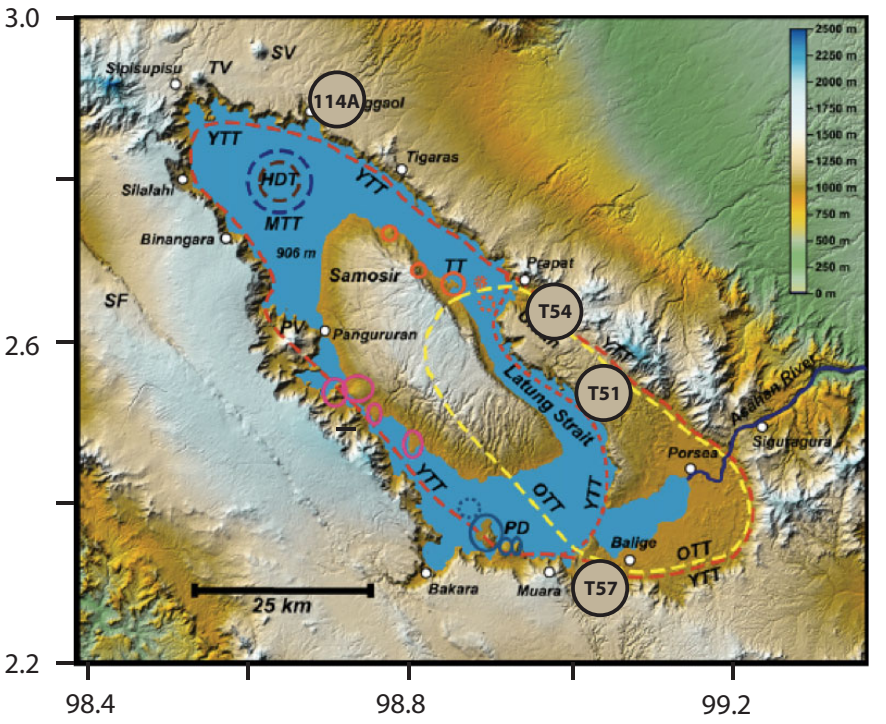

Figure 1. Map showing Toba Caldera Complex, inferred caldera boundaries, and sample locations. YTT: 74 ka Youngest Toba Tuff; MTT: 501 ka Middle Toba Tuff; OTT: 840 ka Oldest Toba Tuff; HDT: 1.2 Ma Haranggaol Dacite Tuff. Samples T51, T54, and T57 are from Craig Chesner and from near the inferred caldera boundaries of the OTT; samples L114A and L349 are from Mary Caress and from near HDT/MTT and an unknown location, respectively. See *Chesner* [2012] for further details about the complex.

heterogeneity records evidence for diverse melt compositions at least thousands to tens of ka before eruption [*Vazquez and Reid*, 2004] but overall compositional heterogeneity of the YTT could have arisen by backmixing during intrusion of less evolved magmas in the lead-up to eruption [*Matthews et al*., 2012; *Vazquez and Reid*, 2004]. Accordingly, the longevity of chemical zoning and its relation to magma storage is unknown.

Zircon geochronology and trace element chemistry can provide tiny but powerful windows into the duration and continuity of magma assembly in the build up to a supereruption like the YTT. The relatively low magmatic temperatures and slightly peraluminous nature of YTT melts means that zircons would have persisted through fluctuations in magma storage conditions [*Miller et al*., 2003]. Zircon also tends to have a strong affinity for the liquid phase because of its small size [*Reid et al*., 1997; *Bachmann and Bergantz*, 2004; *Claiborne et al*., 2010; *Stelten et al*., 2015]. Of particular interest is, therefore, whether YTT zircon crystals reveal evidence for the timing of compositional zoning and its relation to magma storage, a possibility that has heretofore not been tested in zoned rhyolitic systems.

We investigated the record of zircon crystallization across the entire compositional spectra of the YTT magma reservoir, including a rare dacite that might be representative of parental melts. Given the YTT's relative youth, likely complex record of assembly, and possibly plentiful older Toba Caldera Complex-related antecrysts available for recycling, we employed both spatially sensitive U-Th disequilibrium and U-Pb spot and depth-profiling analyses. We find that an appreciable fraction of YTT zircons nucleated prior to the penultimate caldera-forming event 501 ka ago. Zircon growth was protracted and episodic at intervals of ~100 ka, likely because of cycles of thermal rejuvenation and stagnation. The lack of an orderly association of zircon age or composition with host rock composition could reflect zircon's unique ability to be retained in and migrate with melts, likely coupled with extensive crystal mixing and dissolution of major phases (e.g., sanidine, quartz, and biotite) during remobilization episodes. The latest episode of rejuvenation occurred within a few tens of ka of eruption, when crystals were aggregated into the chemically distinct magmas that erupted.

2. Brief History of the Toba Caldera Complex

Northern Sumatra's Toba Caldera Complex has been the locus of silicic volcanic activity for at least 1.3 Ma (Figure 1) [*Yokoyama and Hehanussa*, 1981]. The 2800 km^3 of nonwelded to densely welded ignimbrite and coignimbrite ashfall associated with the YTT exceeds the combined volume of ignimbrite and ash deposits from the three preceding ignimbrites (the ~1.2 Ma ~35 km^3 Haranggaol Dacite Tuff, the 0.84 ± 0.03 Ma ~500–2300 km^3 Oldest Toba Tuff, and the 0.501 ± 0.005 Ma ≥60 km^3 Middle Toba Tuff) [*Nishimura et al*., 1977; *Knight et al*., 1986; *Diehl et al*., 1987; *Chesner et al*., 1991; *Chesner*, 2012]. An astronomically calibrated $^{40}Ar/^{39}Ar$ age of 73.88 ± 0.32 ka (1 σ) [*Storey et al*., 2012] and an inverse $^{40}Ar/^{39}Ar$ age isochron of 75.0 ± 0.9 ka (1 σ, full external errors) [*Mark et al*., 2013] for distal deposits are consistent with prior YTT dating results [*Ninkovich et al*., 1978; *Chesner et al*., 1991].

3. Samples and Analytical Methods

Sample selection was based on mineralogy and crystal content with the intent of sampling the compositional variability and geographic extent of the pyroclastic outflow sheet surrounding Toba caldera (Figure 1). Except for sample T54, which is a welded portion of the ignimbrite [*Chesner*, 1998], all samples represent individual pumice blocks. One sample is a streaked pumice consisting of light colored (L349L) and dark colored (L349D) portions. Aliquots of previously uncharacterized samples were analyzed by X-ray fluorescence for major, minor, and trace element compositions by the GeoAnalytical Laboratory at Washington State University [*Johnson et al*., 1999]. Thorium isotope and U and Th concentrations were obtained by thermal ionization mass spectrometry [*Bohrson and Reid*, 1998]. Glasses and whole rocks powders were digested at 250°C using Teflon Parr bombs in order to ensure complete dissolution. U-Th-Pb isotope compositions of zircon crystals separated by crushing, sieving, and gravity separation and mounted in epoxy were measured using the CAMECA ims 1270 ion microprobe at UCLA [*Reid et al*., 1997; *Schmitt et al*., 2003]. U-Pb analyses included but were not limited to defining dates for grain domains where $^{230}Th/^{238}U$ ratios were within uncertainty of secular equilibrium. *Spot* analyses were performed on zircon crystals from six samples, with grains polished to reveal their interiors. Depth-profiling analyses were performed on zircon crystals from a low-silica and a high-silica pumice block (69.9 and 75.2 wt % SiO_2, respectively). Grains chosen for depth profiling have glass selvages and were mounted in epoxy so that unpolished rims were exposed at the mount surface [*Grove and Harrison*, 1999; *Reid and Coath*, 2000]. Two depth profiles of zircon standard 91500 were also performed in order to assess the depth-dependent reproducibility of this approach. Analysis pit depths were measured with a Dektak® stylus profilometer. In a few cases, the depth profiling was paused at an intermediate depth and the grain polished to the level of the pit floor before recommencing analysis. The ^{238}U-^{230}Th profile of zircon r8g9 was followed by a $^{206}Pb/^{238}U$ profile that began at the base of the former.

4. Results

4.1. Sample Chemistry and Petrography

The relative proportions of YTT magma types have not been documented, but ~three quarters of pumice samples analyzed by *Chesner* [1998] are high-silica rhyolite (73–77 wt % SiO_2); most of the rest are rhyodacite (68–70% SiO_2). Our YTT sample suite spans a large compositional range, from dacite to rhyolite (63–75 wt % SiO_2; supporting information Table S1). Notably, both portions of sample L349 are less silicic than compositions previously reported for the YTT: the dark portion is a low-silica dacite (63 wt % SiO_2) and the light portion is intermediate-silica dacite (65 wt % SiO_2). This sample is otherwise similar in composition to older dacitic rocks from the Toba Caldera Complex.

Salient features of the YTT petrography are summarized in supporting information Table S2. YTT crystal contents range up to 40%, comprising mainly quartz, sanidine, plagioclase, hornblende, and biotite, with subordinate orthopyroxene, allanite, zircon, magnetite, and ilmenite. Hornblende is present in all samples as subhedral to euhedral crystals and is in symplectic intergrowth with orthopyroxene in pumice L349L. Quartz is restricted to samples with >65 wt % SiO_2 and sanidine is restricted to samples with >70 wt % SiO_2. Zircon crystals are mostly euhedral to subhedral, are rimmed by glass, and contain inclusions of glass, magnetite, and euhedral apatite. Most grains exhibit growth zoning and the majority are also sector zoned. Many have

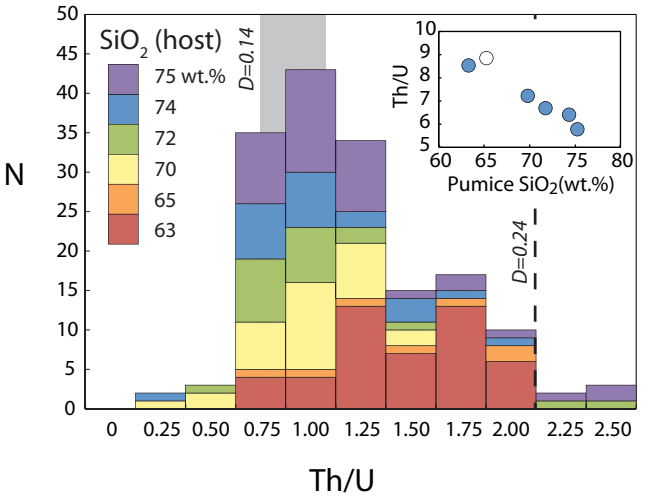

Figure 2. Histogram of zircon Th/U ratios obtained during U-Th and U-Pb spot dating analyses, differentiated according to the composition of the zircon host. Inset shows covariation in Th/U and SiO_2 for whole rocks (closed symbols) and matrix glass (open symbols) (supporting information Table S2). Shaded area: range of Th/U values expected of zircons that grew from rhyodacitic to high-silica rhyolitic YTT melts, as judged by an apparent $D(Th/U)_{zir/melt} = 0.14 \pm 0.02$ obtained for zircon rims in samples T51 and T54. Allowing for zircons that crystallized from dacitic melts and higher values of $D(Th/U)_{zir/melt}$ (up to 0.24) can explain zircon Th/U value that extend to ~2. See text for details. Variations in the Th/U of the depth-profiled 91500 standards varied by <4%, with an overall standard deviation of <1%.

either resorbed cores or growth patterns that are internally truncated. YTT zircon crystals have more melt inclusions and range to lower Zr/Hf than Middle and Older Toba Tuff zircons [*Chesner*, 1998].

YTT whole rock (^{238}U)/(^{232}Th) and (^{230}Th)/(^{232}Th) covary positively, and increase with increasing SiO_2 (supporting information Table S3). Four samples representing the compositional range of the YTT define an apparent isochron of ~190 ka, constrained mainly by sample T54 (supporting information Figure S1). The melt in sample T54 (now preserved as glass) lies on an extension of this array and therefore was not in Th isotope equilibrium with its host at the time of eruption. One other sample diverges to a greater ^{230}Th deficit (L114A), whereas the glass of L349L has a ^{230}Th excess.

4.2. Th/U Variations Within and Between Zircon Crystals

Summaries of zircon spot and depth profile analyses are provided in supporting information Tables S4–S6 and statistical analyses of various aspects of the results are presented in supporting information Table S7. Zircon Th/U is expected to mirror that of the melt from which it crystallizes [*Belousova et al.*, 2002; *Reid et al.*, 2011] and, judging by the range in Th/U spanned by YTT host rocks and matrix glasses (Figure 2 inset), could be expected to decrease twofold with increasing melt SiO_2. For YTT zircons (Figure 2), there is no apparent correlation between average zircon Th/U and host rock Th/U, except that Th/U ratios for zircons from dacitic sample L349D cluster at higher values (average Th/U = 1.4) than the others (average Th/U= 0.97; supporting information Table S4). Th/U ranges defined by zircon populations from individual samples typically span much of the overall range for the zircons, and grain interiors may have higher or lower Th/U than associated rims. Notably, however, rim Th/U ratios in most depth profiled zircons are distinct and cluster at a value of ~0.8 in most T54 grains and around ~1.0 in most T57 grains (supporting information Table S5).

4.3. Zircon Spot Dates

Three types of zircon dates are presented in this and the next section: (1) individual U-Th zircon model crystallization ages obtained by spot analyses, estimated using a variety of proxies for the isotopic composition of the melts from which they crystallized; (2) individual U-Pb zircon dates; and (3) U-Th zircon and, in one case, U-Pb dates obtained by depth-profiles through individual zircons.

4.3.1. ^{238}U-^{230}Th Spot Dates

Ion probe spot analysis of zircon grains yielded cases of both unequivocal ^{230}Th-^{238}U disequilibrium and, for nearly half of the analyses, values within one standard deviation of secular equilibrium (supporting information Table S4 and Figure S1). Model (two-point isochron) zircon crystallization ages [*Reid et al.*, 1997] are reported relative to the isotopic characteristics of the zircons' host rocks and, where available, associated glasses (supporting information Table S3). To allow for zircon crystallization from compositionally diverse melts, a third set of dates was calculated assuming that the melt has (^{238}U)/(^{232}Th) predicted from partitioning relationships, and from excesses of (^{238}U) over (^{230}Th) like those of the whole rocks and glasses on eruption (($^{230}Th/^{238}U$) = 0.9 and 0.84, respectively). These model crystallization ages are somewhat older than those estimated relative to host glass but by only a fraction of the age uncertainty (average of 27% of age

uncertainty except for values within error of secular equilibrium). Dates presented hereinafter are reported relative to whole rock compositions.

Where possible, spot analyses are informally categorized as "rims," "cores," and "interiors" on the basis of their relative proximity to grain centers and rims, as determined by cathodoluminescence imaging (supporting information Table S4). These distinctions are not rigorous because ion probe spots capture a much broader growth cross section when they are located toward a prismatic face rather than along the longitudinal axis. Spot "rim" analyses of YTT zircons yield dates that range from eruption-aged to ~300 ka, averaging ~190 ka (weighted mean; supporting information Table S7). Spot core dates range from ~160 ka to nominal dates of >350 ka (i.e., ^{230}Th-^{238}U effectively in secular equilibrium), averaging ~280 ka older than rims. In more than half of the cases where single grains were analyzed multiple times, domains crystallized more than >100 ka apart. The broadest age distributions and youngest mean dates are observed in the least and most silicic host rocks (Figure 3; supporting information Table S7).

4.3.2. ^{206}Pb/^{238}U Spot Dates

^{206}Pb/^{238}U dates reported here incorporate corrections for common Pb (using a ^{207}Pb-correction) and for ^{238}U-^{230}Th disequilibrium [following *Schmitt et al*., 2003] (supporting information Table S6). Common ^{207}Pb/^{206}Pb is assumed to be 0.834, the average value of two values reported for the YTT rhyolites [*Turner and Foden*, 2001]. A zircon crystal in each of three samples yielded U-Pb dates much older than the 1.3 Ma duration of Toba-related volcanism. Of these samples, only the CL-imaged zoning pattern in the T51 zircon is erratic. An appreciable proportion of the analyzed zircons (~30%) contain domains older than 500 ka, but many analyses performed at or close to locations that yielded ^{238}U-^{230}Th at or near secular equilibrium yielded dates of <450 ka (Figure 3). In most instances where U-Th and U-Pb dating was performed on the same general areas within individual zircons, the results are internally consistent (Figure 4; supporting information Tables S4 and S6).

4.4. Zircon Depth Profile Analyses

Zircon depth profiles performed on four grains from each of samples T54 and T57 confirm that zircons grew at least intermittently over periods of >100 ka (supporting information Table S5). These profiles range from 7.5 to 22 μm in length. T57 zircon r8g9 records the largest variation of dates for the profiled grains, ranging from within error of the 74 ka eruption age at the rim to ~575 ka at ~20 μm depth (Figure 5b). Multiple depth profiles on individual grains (two for T57 grain r8g7 and three for T54 grain r3g4; Table S5) confirm the robustness and variability of the dating profiles. However, the tendency for the first (^{230}Th)/(^{238}U) ratios to be higher than immediately following ones suggests that the most rimward analyses were affected by organic contamination of the mount surface [*Schmitt et al*., 2010]. One zircon crystal from each sample differs from the others in having no indication of growth younger than ~175 ka.

5. Analysis of Results

5.1. Selectivity of Ion Probe Analyses to YTT Zircon Crystallization Ages

Ion microprobe analyses quantize what could be spatially heterogeneous compositional and temporal domains. Spot analyses—because of their size and shape—could not sample in any significant way the outermost (several μm) portions of grains. Depth profile analyses, on the other hand, may not adequately characterize zircon cores. Based on YTT zircon sizes, depth profile analyses mostly characterize the outer ~35% by zircon length or ~70% by volume, and spot analyses mostly characterize the inner half by volume. Depth profiling is also capable of being as much as 2 orders of magnitude more spatially selective than spot analysis [*Grove and Harrison*, 1999; *Mojzsis and Harrison*, 2002; *Trail et al*., 2007; *Storm et al*., 2012], with two important caveats. First, the depth sensitivity depends on the extent to which the ion beam is perpendicular to zircon growth zoning, and on the ideality of the ion probe pit (i.e., its approximation to perfectly cylindrical with a flat bottom). Mixing of different growth zones appears to be minimal in our study judging by the pronounced changes in Th/U (and/or U contents) over ~1 to 1.5 μm in most of the depth profiles (Figure 5). Second, once the diameter of the ionprobe spot exceeds the size of the more coreward domain, the sensitivity of depth profile analysis approaches that of spot analysis. Consequently, spot analyses provide a better assessment of the overall distributions of crystallization ages for cores and interiors, whereas depth profiles are a better source of information about the near-rim portions of the grains.

Several lines of evidence indicate that the range in crystallization ages for YTT zircons does not reflect admixtures of younger growth with ubiquitous xenocrystic domains. If mixed with ~75 ka cognate crystal

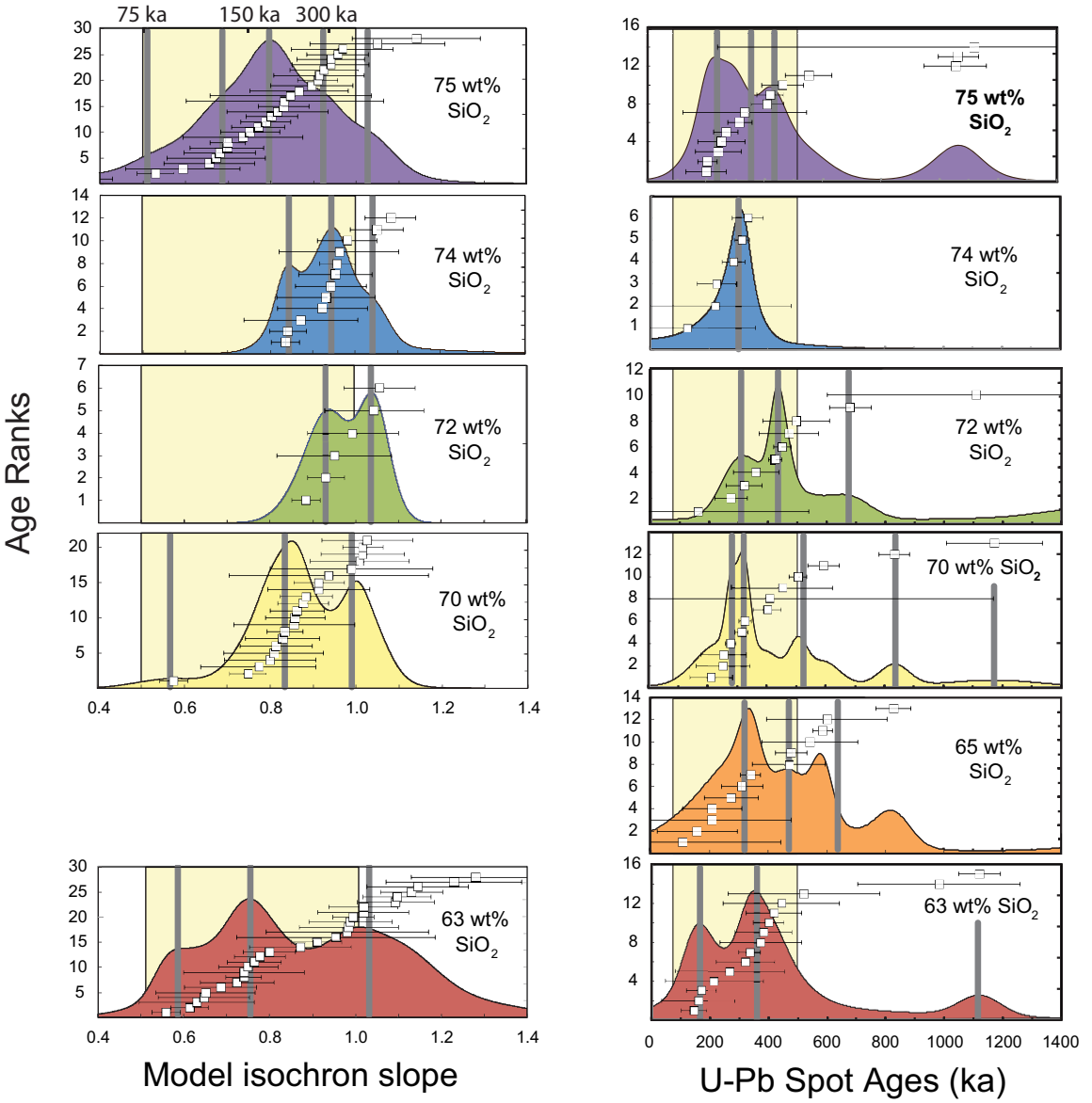

Figure 3. Results of ion microprobe dating of zircons from representative Youngest Toba Tuff pumices and a welded tuff (T54). Probability density population fill colors correspond to SiO_2 of host pumice, and are identical to those in Figure 2. (left column) Distributions of U-Th zircon model ages represented as isochron slopes (proportional to crystallization age) to incorporate errors symmetrically. Rank order plots (errors are 1σ) are superimposed on probability density populations (obtained using Isoplot) [*Ludwig*, 2003]. Light yellow shaded background delimits the range of isochron slopes from the 74 ka eruption age [e.g., *Chesner et al.*, 1991] to secular equilibrium. (right column) Distributions of U-Pb zircon ages for same samples as in left column, with the addition of L349L, shown as plots of rank order and probability density populations. Weighted mean ages and their uncertainties and MSWDs are summarized in supporting information Table S7.

growth, for example, zircon dates of up to 500 ka are permissive of no more than a few percent contribution from a xenocrystic component like that of the youngest xenocryst (~20 Ma), even if xenocrysts have significantly lower U contents and associated radiogenic daughter ^{206}Pb (Figure 4). Such small contributions could not explain the intermediate ages that persist over several micrometers in the depth profiles or account for the accompanying Th/U changes (Figure 5). Additionally, ^{238}U-^{230}Th-^{206}Pb characteristics of mixtures between young zircons and xenocrysts will fall along linear trends that are discordant to the concordia defined by two-point ^{230}Th-^{238}U isochron slopes and $^{206}Pb/^{238}U$ dates (Figure 4). The broadly concordant U-Th and U-Pb dates for the YTT zircons indicates that, even though individual xenocrysts are members of the zircon population, they do not account for the distribution of crystallization ages that characterizes most YTT zircons.

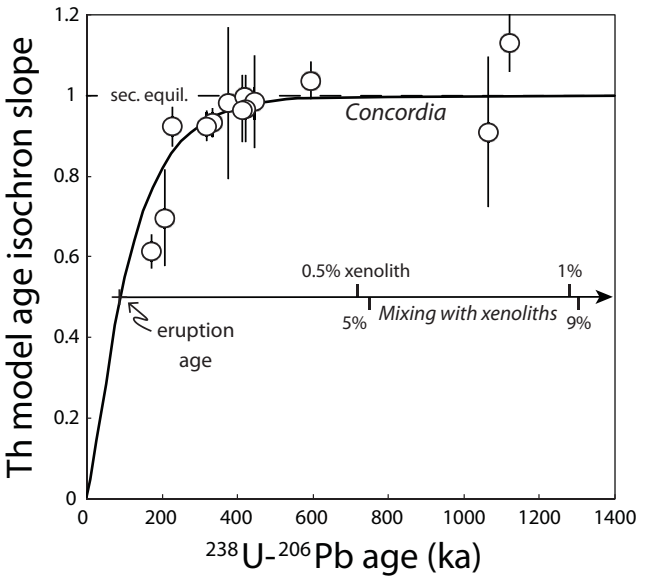

Figure 4. Graph pairing model age ^{238}U-^{230}Th isochron slopes and $^{206}Pb/^{238}U$ ages, where both analyses were performed on the same areas of individual zircons. The concordant age information can best be explained by radiogenic ingrowth. Shown for reference is an example of a mixing array between cognate zircon growth and a 20 Ma xenocrystic domain contribution. Labeled tic marks show proportions of xenocryst in the mixture if U concentration of xenocryst is similar to that of cognate zircon (upper tic mark) or a factor of 10 lower (lower tic mark). Small age discordances could however be explained by analytical hybridization between <500 ka age domains.

5.2. YTT Zircons Mostly Nucleated and Grew Since the Last Caldera-Forming Eruption

Zircon population density distributions for all U-Th and U-Pb spot dates are summarized in Figure 6, along with the means for those dates that fall in the Middle Toba Tuff (MTT)-YTT repose interval; these are dominantly for zircon interiors and cores. Although the overall distribution of U-Pb dates might be inferred to be somewhat older overall than that of the U-Th dates, it is important to consider that: (1) dates greater than ~300 ka are almost invariably within error of secular equilibrium and unresolvable by U-Th analyses; (2) U-Pb analyses were performed preferentially on grain domains which, based on their U-Th results, were found to be close to or within error of secular equilibrium; and (3) the resolution of U-Pb dates at the younger end of the crystallization age spectrum can be poor due to relatively low U concentrations in YTT zircons.

Spot analyses show that the interiors of most YTT zircons grew ~100–400 ka before eruption. Judging by the crystallization ages recorded by crystal cores, which provide insights into the timing and frequency of crystal nucleation and initial growth, zircons nucleated at various times before but mostly after the MTT eruption (supporting information Tables S4 and S6). Depth profile results yielded similar results and notably, U-Pb dates of ~575 ka obtained on the deepest T57 profile and within error of ~500 and ~800 ka on three others. Nucleation may have been discontinuous, and there is no statistically significant correlation between core crystallization ages and zircon size, in contrast to what is expected for zircons that progressively nucleated and grew from melts.

5.3. YTT Zircons Grew Episodically

Several lines of evidence suggest that YTT zircons comprise multiple crystallization age populations: (1) The mean square of the weighted deviates (MSWD) are greater than expected for a single population, even when grains older than the MTT are excluded (Figure 6; supporting information Table S7). (2) Peaks in the population density distributions of the crystallization ages suggest that zircon growth may have been periodic. (3) Stepwise changes in age within depth-profiled zircons further suggest that crystallization progressed in a discontinuous fashion. Thus it appears that either blooms in YTT zircon crystallization occurred episodically or zircons were periodically remobilized into an environment favorable for crystallization.

A mixing modeling algorithm was applied to quantify the distributions of spot dates [*Sambridge and Compston*, 1994]; the results are summarized in supporting information Table S7. Multiple populations of dates for all samples are indicated by the distribution of U-Th model isochron slopes (used instead of dates because of the latter's asymmetrical uncertainties) and $^{206}Pb/^{238}U$ dates (Figure 3). Small peaks in crystallization age correspond to the timing of previous eruptions (e.g., MTT and OTT) or predate them (peaks at ~680 and ~1090 ka, respectively). The youngest peak ages are observed in the least and most evolved samples. Populations at intervals of ~100 ka are observed in the U-Th and U-Pb date distributions of two or more samples (~80–90, ~190, and ~300, and ~310 and ~430 ka, respectively; supporting information Table S7). When the zircon populations are treated as a whole, the same peaks in crystallization ages are apparent, with the ~300 ka peak well represented by both U-Th and U-Pb dating.

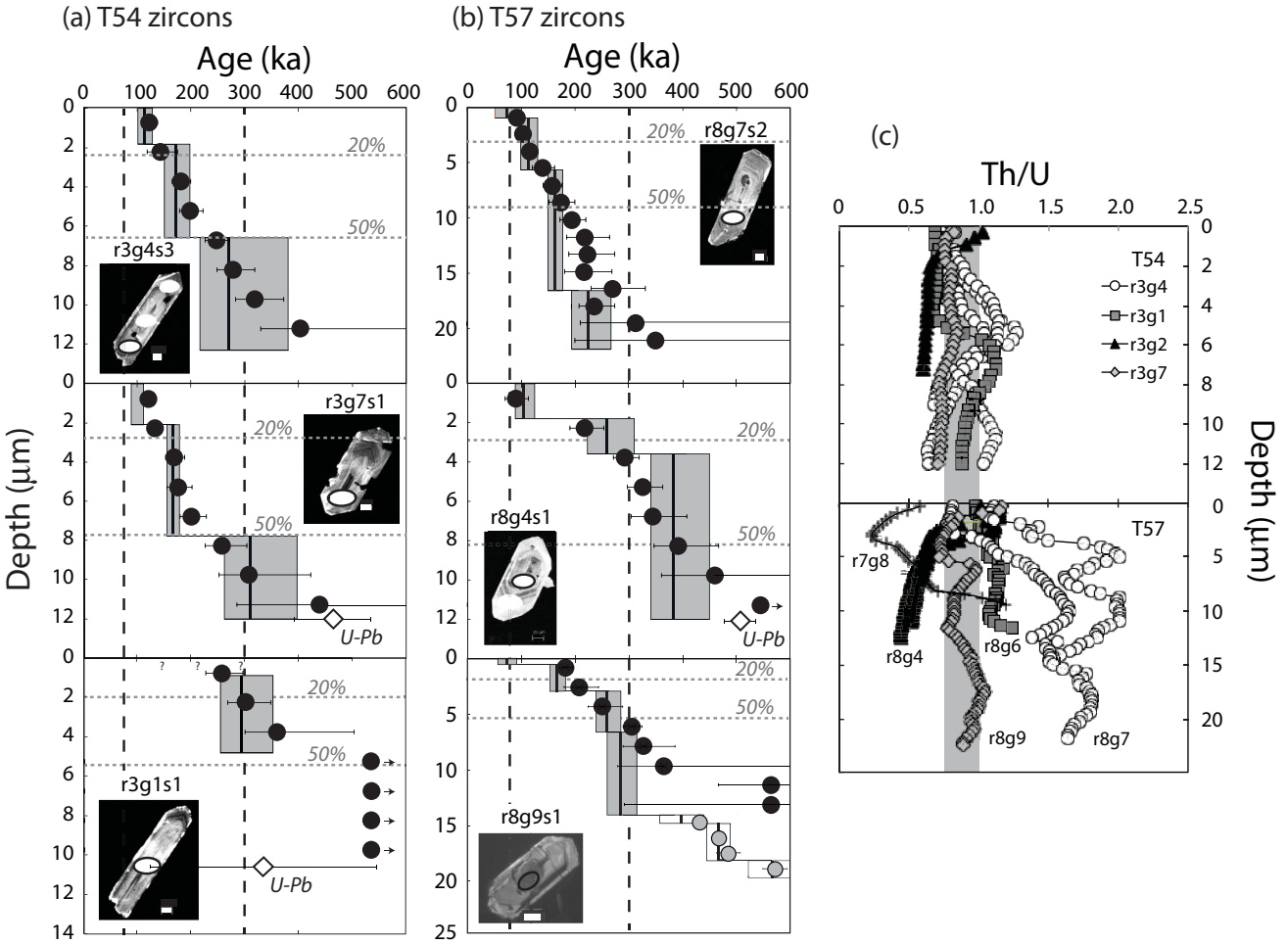

Figure 5. Results and models of representative ion microprobe depth profiles of Youngest Toba Tuff zircons (see supporting information Table S3 for data summary). Sputtered depths determined using a Dektak® stylus profilometer. Also shown are cathodoluminescence images of grain interiors at depths of pit bottoms after grinding and polishing, and analysis locations; white scale bar represents 20 μm. Age distribution models for grains from samples (a) T54 and (b) T57. Circles are the results of Bayesian stratigraphic modeling and gray boxes are the results of successively combining blocks of data within MSWD constraints (dark vertical line represents mean age and width of box represents 1σ asymmetric error; see text for details). Diamonds show U-Pb dates obtained on grain interiors. Vertical dashed lines signify eruption age (74 ka) and a reference 300 ka age which approaches the practical upper limit of resolvable U-Th ages. Results for the zircons in first row of figures suggest that they might have grown semicontinuously whereas those in the second row have clearer evidence of crystal growth hiatuses. Near eruption-aged growth was not detected on some grains like T54 zircon r3g1 (row 3) which has a step-like near-rim Th/U plateau like that expected from near-rim growth: in these grains ^{230}Th may have been contaminated by epoxy. At the other extreme, U-Pb depth profiling of the interior of T57 grain r8g9 shows that growth occurred as early as >500 ka ago. No evidence of ^{238}U-^{230}Th disequilibrium was detected in one of the grains that are not shown (T54_r3g2s1). (c) Variation in Th/U with depths in T54 and T57 zircons. Shaded area shows range expected for growth from melts with compositions like YTT whole rocks and glasses.

Two types of modeling were applied to better understand the internal distributions of crystallization ages for the depth-profiled grains, where successive blocks of dates can overlap in their errors. Resulting dates and uncertainties are shown in Figure 5 and summarized in supporting information Table S5. In the first approach, the stratigraphic modeling of Isoplot v. 4.15 [*Ludwig*, 2003] was used. This method employs the "stratigraphic" constraint that age increases inward in a zircon and uses a Monte Carlo implementation of Bayesian statistics. In the second approach, the results from individual data blocks were binned together to yield dates spanning greater depth intervals. Dates were calculated iteratively by successively adding blocks to the weighted mean, beginning with the most rimward block of data. For a single crystallization age population, the MSWD is expected to generally approach unity as more data are added. At various points in the depth profiles, the MSWD increasingly diverged from unity instead. Where such inflections occur, succeeding data blocks were binned as a different age population and data blocks associated with the inflection distributed between the two age populations.

Stratigraphic modeling of the U-Th-Pb characteristics of individual YTT zircons is suggestive of semicontinuous growth of most zircon crystals for periods of 200 ka and longer (supporting information Table S5).

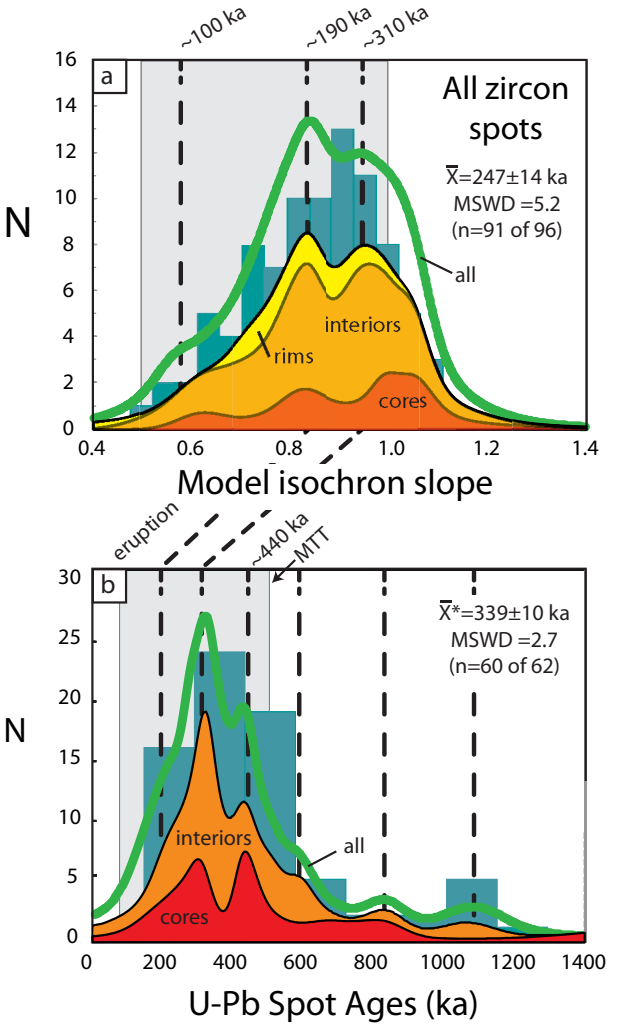

Figure 6. Probability density diagrams summarizing (a) spot U-Th model-age isochron slopes and (b) all U-Pb ages. The duration of the MTT-YTT repose interval (501–74 ka) is shown by the gray-shaded area. U-Th model-age isochron slopes and U-Pb dates are divided into four (U-Th) and three (U-Pb) populations: all zircon and, for those zircon for which locations within grains are known, cores, interiors, and rims (see text for further information). Mean ages, uncertainties (1σ), and MSWDs also presented, which, for U-Pb dates ($\bar{X}$*), are only for those within uncertainty of the MTT-YTT repose interval (>75% of all U-Pb dates). For all U-Pb dates within uncertainty of the lifetime of the Toba Caldera Complex, the mean U-Pb age is only slightly older at 356 ± 12.5 ka (MSWD = 4.5; n = 69 of 80). Mixture modeling of U-Th and U-Pb dates [*Sambridge and Compston*, 1994] suggests the presence of at least four episodes of post-MTT zircon growth (~100, ~190, ~310, and 440 ka; indicated by dashed vertical lines); additional peaks may be present (Figures 3 and 9; supporting information Table S7). For data sets of this size, an age population composing >10% of the overall YTT population should have been detected at the 95% confidence limit [*Dodson et al.*, 1988]. Short-dashed lines connecting two figures tie similarly aged clusters determined by both U-Th and U-Pb dating. A complete summary of the distributions of age populations is given in supporting information Table S7.

Linear growth rates estimated from these crystallization age distributions average $1.4 \pm 0.6 \times 10^{-16}$ cm^2/s, within the range of estimated zircon growth rates (10^{-15}–10^{-19} cm^2/s) [*Watson*, 1996]. Breaks in slope are also permissive of age clustering (Figures 5a and 5b). Mixture modeling of the "stratigraphic ages" suggests peaks in growth at ~130, ~165, ~210, and ~300 ka (Table S7). Age domains in zircons from low-silica rhyolite (T57) obtained by sequential age binning cluster at ~160, 250, and 360 ka (Figure 5b); in high-silica rhyolite zircons (T54), they cluster at ~175 and 240 ka (Figure 5a), statistically indistinguishable from the populations in T57, but the older cluster may, judged by the stratigraphic ages clustering, be a mixture of ~200 and ~274 ka ages. Not all age zones are present in all grains. "Missing" age zones could, nevertheless, be present but not resolved by age binning or, for older zones, because the depth profiles were too short to detect them. In general, it appears that zircons with cores >300 ka in age experienced progressively younger growth, growth that may have been more pronounced at ~170 ka and closer to eruption.

5.4. Melts Responsible for YTT Zircons are Diverse in Composition

Zircon rims are only 1–2 μm thick in most cases, judging by the clustering of composition and crystallization ages, and mantle older episodes of growth characterized by different Th/U signatures. Because Th^{4+} and U^{4+} are isovalent and similarly sized, a zircon's Th/U ratio may faithfully track the compositions of melts from which it crystallized [*Belousova et al.*, 2002; *Reid et al.*, 2011]. Using host glasses as a melt proxy and data for zircons that have near eruption-aged growth, apparent D(Th/U) (zircon/melt) values for T57 (0.14 ± 0.02) and T54 (0.15 ± 0.02) are remarkably similar and consistent with values of D(Th/U) = 0.14–0.17 reported elsewhere [*Schmitt et al.*, 2003; *Blundy and Wood*, 2003; *Stelten et al.*, 2015]. This agreement shows that many YTT zircons grew from melts like those of their host melts within tens of ka of eruption.

Normal zoning should, judging by chemical variations defined by YTT pumice compositions (supporting information Table S1), be recorded as a decrease in zircon Th/U, likely as a result of co-precipitation with

allanite [*Chesner and Ettlinger*, 1989; *Hermann*, 2002; *Vazquez and Reid*, 2004]. Zircon that nucleated from the least evolved YTT sample, dacite L349D, should have Th/U in the range of 1.3–2.1 for the more generous estimates for D(Th/U) of 0.14–0.24 [*Schmitt et al*., 2003]. The distinctly larger population of high Th/U grains in sample L349D (Figure 2) therefore suggests that its zircons could be mostly cognate to their host rock, with values lower than ~1.3 explained by progressive growth ± nucleation as the residual liquid evolved. Zircon domains from the other samples only occasionally have Th/U values expected for crystallization from dacite; instead they mostly appear to have crystallized from more evolved magmas. Thus, in general, those domains with Th/U ≥ 0.73 could have crystallized from melts delimited by YTT whole rocks and matrix glasses (Th/U ≥ 5.2) [*Chesner and Luhr*, 2010; this study], assuming D(Th/U) ≥ 0.14 (Figure 2). Others, approximately a quarter of the analyzed zircon domains, appear to have crystallized from melts more evolved than this. A few cores or interiors of grains do not conform to the foregoing generalizations and have high Th/U but also high U contents or U secondary ion beam intensities; they could have crystallized in oxidized hydrothermal and/or vapor phase environments [*Schmitt*, 2006; *Bacon et al*., 2007].

Finally, we note that there is no clear correlation between host rock compositions, and zircon core and interior domain compositions, in contrast to expectations for crystals cognate to their hosts. More generally, there is no overall secular chemical trend in zircon Th/U (Figure 7): the same age populations are represented in the compositional groups as in the overall age data, and a range in composition is present at each interval identified by mixture modeling (supporting information Table S7) [*Sambridge and Compston*, 1994]. Depth profiles show that Th/U zoning within individual grains can be at least locally reversed or oscillatory (Figure 5c). Some of these changes could reflect variations in zircon's stability relative to allanite (the phase that mainly controls Th/U fractionation) due to spatial and/or temporal heterogeneities in p_{H2O}, as also proposed for the Bishop Tuff [*Reid et al*., 2011]. Analyses of other zircon-specific proxies for differentiation, e.g., Eu/Eu* and Zr/Hf, could independently test this possibility. The depth profiles also confirm that the compositional range exhibited by individual grains spans a limited portion of the population's compositional range. Compositions collectively scatter most between the various core domains and least between the (few in number) rim analyses in each sample. This suggests that crystals nucleated from a host of melts, mostly ranging in composition from low- to high-silica rhyolite, before being aggregated into and growing in new chemical domains, sometimes several times, and finally being entrained in the dominantly rhyodacitic to rhyolitic composition magmas that erupted.

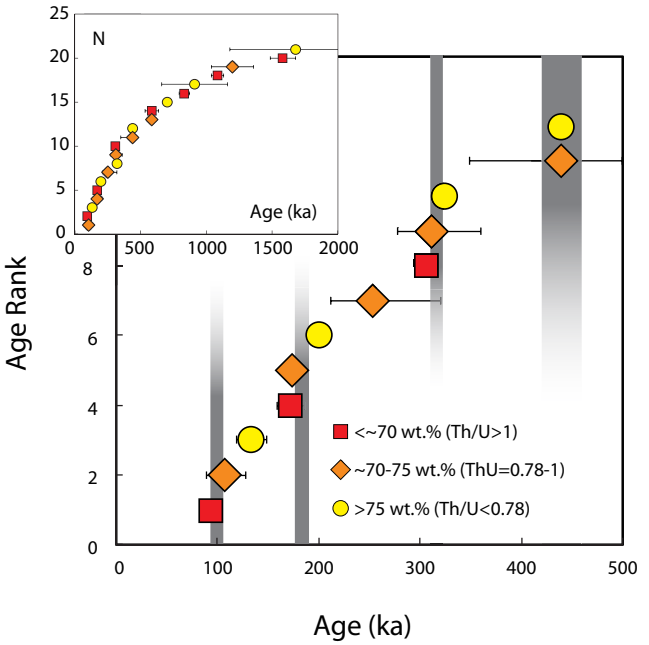

Figure 7. Age rank diagram showing dates of zircon crystallization ages of three populations clustered according to Th/U, which are expected to reflect differences in host compositions, as identified by mixture modeling [*Sambridge and Compston*, 1994]. No evidence of a secular chemical change in magma responsible for zircon crystallization is observed, and vertical lines (also identified by mixture modeling) show that zircons may have crystallized from diverse magma compositions within relative short periods of time. Age uncertainties are 1σ. Age population results are summarized in supporting information Table S7.

6. YTT Zircons Grew in a Low-Pressure, Compositionally Heterogeneous Magmatic System

6.1. Conditions of Zircon Growth

An appreciation for the relation of zircon crystallization ages to magmatic processes requires an understanding of the magmatic conditions indicated by the occurrence of zircon. The subchondritic and variable Zr/Hf (19–30) that accompanies high and relatively constant SiO_2 in YTT matrix glass and melt inclusion compositions show that melts evolved in equilibrium with

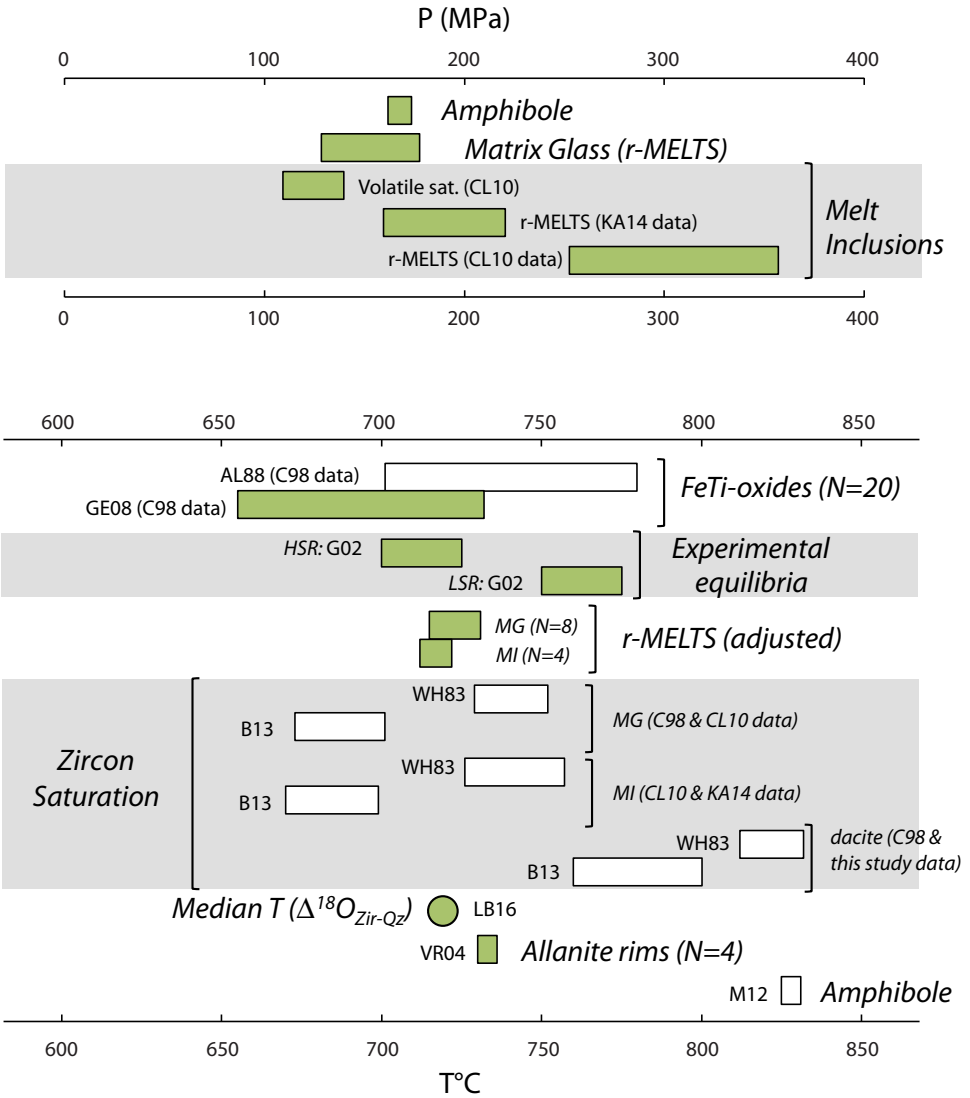

Figure 8. Pressure and temperature estimates for mineral and melt equilibria in the Youngest Toba Tuff. Abbreviations are: high-silica rhyolite, HSR; low-silica rhyolite, LSR; matrix glass, MG; melt inclusions, MI. Raw data sources are: *Chesner* [1998] (C98); *Chesner and Luhr* [2010] (CL10); and *Kularatne and Audétat* [2014] (KA14). Rhyolite-MELTS temperatures have been adjusted downward by 40°C (see text for details). Additional references, mainly models for or results of thermometers and barometers, are—AL88: *Anderson and Lindsley* [1988]; B13: *Boehnke et al.* [2013]; G02: *Gardner et al.* [2002]; GE08: *Ghiorso and Evans* [2008]; LB16: *Loewen and Bindeman* [2016]; M12: *Matthews et al.* [2012]; WH83: *Watson and Harrison* [1983]; VR04: *Vazquez and Reid* [2004].

zircon at the haplogranitic eutectoid, and therefore at low-pressure conditions [*Blundy and Cashman*, 2001; *Claiborne et al.*, 2006; *Gualda and Ghiorso*, 2013]. In addition, Zr/Hf ratios in quartz-hosted melt inclusions (23–28) are positively correlated with CaO (0.6–0.8 wt %), Eu/Eu* (0.02–0.24), and Nd/Yb (2.7–4.9) (data of *Chesner and Luhr* [2010]). This variability shows that, in addition to quartz, zircon was co-crystallizing with plagioclase (CaO control), sanidine (high D_{Eu} compared to Sm and Gd) and likely allanite (high $D_{Nd/Yb}$). It appears, therefore, that significant YTT zircon crystallization occurred in the upper crust.

Figure 8 summarizes pressure and temperature estimates for the YTT obtained through a variety of approaches. Several lines of evidence (phase equilibria, melt inclusion volatiles, and minimum melt compositions) suggest crystallization pressures of 110–180 MPa [*Gardner et al.*, 2002; *Chesner and Luhr*, 2010; *Gualda et al.*, 2012b; *Matthews et al.*, 2012; *Gualda and Ghiorso*, 2014]. At these pressures, quartz and two-feldspar saturation is expected to occur at T ~700–725°C, judging by experimental results for a water-saturated high-silica YTT rhyolite [*Gardner et al.*, 2002] (Figure 8). Somewhat higher temperatures could apply for quartz-plagioclase saturation in low-silica rhyolite, if pumices of this type are not appreciably

influenced by crystal accumulation. When rhyolite-MELTS simulations are applied to the experimental glasses, they yield melt equilibration temperatures ~25–60°C higher than those of the experiments responsible for the glasses, in keeping with other observations that r-MELTS overestimates temperatures by 30–40°C [*Gualda et al*., 2012a; *Gardner et al*., 2014]. Therefore, the narrow range of temperatures estimated for multiphase saturation of matrix glasses from diverse YTT host rocks (713–730°C; Figure 8) are those adjusted downward by 40°C from simulated values. Zircon saturation temperatures, T_{ZS}, for matrix glasses are somewhat lower and higher than the foregoing, when estimated using the calibrations of *Boehnke et al*. [2013] and *Watson and Harrison* [1983], respectively (Figure 8). These "quench" T_{ZS} are mostly correlated with matrix glass CaO (data of *Chesner and Luhr* [2010]) and could signify a preeruption or syn-eruption thermal gradient of ~30°C. Both experimental and model temperatures fall within the wide range of FeTi-oxide "eruption" temperatures (calibration of *Ghiorso and Evans* [2008]). Collectively, magmatic conditions at the time of eruption were shallow, cool, and relatively wet, conditions favorable for zircon preservation [*Ellis et al*., 2014; *Lipman and Bachmann*, 2015].

Estimates of major phase growth conditions prior to eruption are also shown in Figure 8. Not surprisingly, given their compositional similarity to matrix glass, melts trapped within quartz [*Chesner and Luhr*, 2010; *Kularatne and Audétat*, 2014] overlap in their corrected r-MELTS temperatures. Lower SiO_2 contents in some melt inclusions compared to matrix glass (data of *Chesner and Luhr* [2010], but not *Kularatne and Audétat* [2014]) could indicate inclusion entrapment pressures ~100 MPa higher than inferred for matrix melts as well as those experimentally constrained [*Gualda and Ghiorso*, 2014], but the SiO_2 difference could alternatively be explained by effects associated with syn- (i.e., boundary layer) or postentrapment quartz growth. Also, potentially related to melt entrapment are Zr contents that correlate positively with those of incompatible elements, the opposite of what would be expected for progressive melt evolution. If only the results of *Kularatne and Audétat* [2014] are considered, a narrow range of T_{ZS} that lies within the range estimated for matrix glasses and from experimental equilibria is found (Figure 8). Also in agreement with these temperature estimates is a median value of 719°C for oxygen isotope equilibration between quartz and zircon [*Loewen and Bindeman*, 2016]. At variance with these are temperature estimates of >820°C for YTT amphibole crystallization [*Matthews et al*., 2012] and >760°C for zircon saturation in dacites associated with the Toba Caldera Complex. If dacitic magmas are parental to the YTT system, r-MELTS simulations suggest that zircon saturation might be achieved once liquids evolve to Zr contents and lower temperatures like those of the rhyodacites (7–8% crystallization). In this case, the temperature of first zircon saturation could also be >820°C.

The Ti contents of quartz (TitaniQ thermobarometer) [*Wark and Watson*, 2006] should be able to provide insight into the evolving nature of zircon crystallization conditions, but the picture for YTT quartz is complicated by uncertainties in $a\mathrm{TiO_2}$ and the pressure dependence of the thermometer calibration [*Huang and Audétat*, 2012; *Thomas et al*., 2010, 2015], as we briefly illustrate here. Rims of some Toba quartz exhibit at least a twofold increase in Ti contents over those of quartz cores, which could be evidence of a temperature increase and/or an increase in $a\mathrm{TiO_2}$ associated with magma recharge during the final ~100 years before eruption [*Matthews et al*., 2012]. Higher $a\mathrm{TiO_2}$ estimated from FeTi-oxide equilibria (0.55) than from melt inclusions (0.21–0.28) [*Kularatne and Audétati*, 2014] would seem to favor the latter interpretation and suggests an insignificant temperature increase. On the other hand, the lower estimates for $a\mathrm{TiO_2}$ values rely on zircon saturation temperatures, and the differences in apparent $a\mathrm{TiO_2}$ disappears if the zircon saturation calibration of *Boehnke et al*. [2013] is used instead of *Watson and Harrison* [1983]. Furthermore, if crystallization P is taken to be ~150 MPa, the thermobarometer calibration of *Huang and Audétat* [2012] yields rim crystallization conditions of <785°C if $a\mathrm{TiO_2} \geq 0.55$, broadly consistent with those expected. If the calibrations of *Thomas et al*. [2010, 2015] are applied instead, reasonable quartz rim temperatures of 705–750°C are obtained for the same pressure conditions only when the lower estimate of 0.21 for $a\mathrm{TiO_2}$ is used. Consequently, Ti-in-quartz constraints on crystallization conditions cannot presently provide definitive insights into the conditions that accompanied zircon crystallization.

6.2. Zoning of the YTT Magmatic System: Top-Down or Bottom-Up?

The nearly identical bulk compositions of matrix glasses from pumices of diverse compositions [*Chesner*, 1998] require magma reservoir liquids to have equilibrated at roughly similar conditions before quenching on eruption. Correspondingly, the covariation between whole rock composition and crystal content could be explained by original melt heterogeneity, whereby more evolved magmas are expected to be less crystalline compared to less evolved ones when equilibrated at similar conditions, or by two-phase behavior

leading to domains of crystal loss (high-silica rhyolite) and accumulation (low-silica rhyolite). *Chesner and Luhr* [2010] attempted to distinguish between these possibilities by observing that melt inclusions in quartz from both low- and high-silica YTT pumices are SiO_2 rich (74.5–77 wt % SiO_2). From this, they concluded that parental YTT liquids were initially high-silica rhyolite, and that low-silica rhyolites were produced as crystals accumulated by settling. This interpretation does not strictly follow because, as expected from phase relations [*Blundy and Cashman*, 2001; *Gualda and Ghiorso*, 2014] and as shown experimentally for the YTT [*Gardner et al*., 2002], quartz cannot begin to crystallize from YTT melts until host liquids evolve to high-silica compositions, even if melts are initially much lower in silica. Quartz-hosted melt inclusions necessarily can only provide insights into YTT magma evolution after the liquids become quartz-saturated.

Heterogeneity was present within the YTT magma reservoir at the time of eruption, despite bulk liquid compositions that are largely buffered at the eutectoid. This diversity is evident from matrix glass variability in minor elements (e.g., CaO, FeO, and TiO_2) and trace element ratios (e.g., Th/U: 5.3–9.0; Zr/Hf: 22–34; Eu/Eu*: 0.13–0.64; and Nd/Yb: 4–11; data of this study and *Chesner and Luhr* [2010]) that correlate with whole rock compositions. Compositional variability of glasses from proximal and distal YTT pyroclasts has been documented by other studies [e.g., *Gatti et al*., 2014; *Westgate et al*., 2013]. Mineral assemblages and crystal compositions are also linked to host rock compositions, a feature that could be reconciled with progressive "top-down" crystal settling if sequential mineral equilibrium with evolving liquids is recorded in the cumulate pile. An alternative interpretation for this zoning may be "bottom-up" mixing with less evolved melts introduced at the base of the magma reservoir. Trace element covariations could be at least partially produced by mineral dissolution or by mixing with melts produced at least partially within a cumulate pile that acted as a barrier to ascent of recharge melts [*Wark et al*., 2007; *Wolff et al*., 2015]. New liquids produced in this way could fractionate crystals that then, in turn, undergo an additional round of melting.

There are features of the YTT that support a role for bottom-up development of zoning. Titanium-rich rims on YTT quartz have been interpreted to record the effect of magma recharge [*Matthews et al*., 2012], as noted above. Whereas an increase in $a\mathrm{TiO_2}$ or temperature, or a decrease in $a\mathrm{H_2O}$ or pressure, could independently or collectively produce Ti-rich rims, the fact that the Ti-rich rims mantle and truncate zoning in well-rounded quartz grains favors formation of the rims after a heat influx. Low-silica rhyolites with the highest Ba contents lack sanidine, a feature that is difficult to explain by crystal accumulation. The Ba- and Sr-rich nature of matrix glasses compared to glasses entrapped in quartz in the low-silica rhyolites would be also consistent with a scenario of "bottom-up" zoning: melts could remain persistently in equilibrium with quartz and melting of sanidine-bearing cumulates would result in Ba enrichments [*Wolff et al*., 2015]. The nearly twofold greater Eu/Eu* of matrix glass from low-silica rhyolite L114A (this study) compared to matrix glasses analyzed by *Chesner and Luhr* [2010] may also require a contribution from sanidine remelting. The approximately threefold range in Zr contents between different pumices (105–265 ppm; supporting information Table S1) is permissive of the possibility that low silica rhyolite pumices accumulated zircons, but chondritic to subchonodritic Zr/Hf (23–36) [*Chesner and Luhr*, 2010; *Deering and Bachmann*, 2010] suggest that compositional heterogeneities could be the result of recharge after zircon fractionation. Quartz-hosted melt inclusions also exhibit higher compatible element concentrations nearer to quartz rims, a feature that could be explained by magma recharge accompanied by quartz crystallization, but has elsewhere been interpreted to record settling of crystals into less silicic melt [*Chesner and Luhr*, 2010]. Strontium isotope disequilibrium between glass and minerals is also evident [*Chesner*, 1988] and, because $^{87}Sr/^{86}Sr$ ratios are lower in groundmass glass than their host whole rocks, the opposite of what would be expected of progressive assimilation but permissive of recharge by less contaminated melts.

7. The Complex and Disparate Crystal Records of the YTT Reservoir

7.1. Protracted and Episodic Growth of YTT Zircons From Diverse Melts

Zircon xenocrysts are generally rare in silicic volcanic systems, as most recently summarized by *Cooper* [2015]. The paucity of xenocrysts in the YTT is nonetheless notable because relatively old crustal materials clearly played an important role in melt genesis, judging by the rhyolites' radiogenic $^{87}Sr/^{86}Sr$ (0.7134–0.7140), high $\delta^{18}O$ (generally $+9.2$ to $+10.7$), and low ε_{Nd} (-10) [*Chesner*, 1988; *Turner and Foden*, 2001; *Bindeman and Simakin*, 2014]. Crustal contributions to the YTT, which might have included several kilometers-thick Paleozoic metasedimentary basement [*Aldiss and Ghazali*, 1984], were apparently

incorporated without significant entrainment of zircons and/or country rock zircons were nearly quantitatively resorbed during crustal melting. In the first case, zircon crystals would not have been efficiently entrained during anatexis and melt extraction; in the second, melting would have proceeded at relatively high temperatures. Conditions for both could pertain to the lower crust. Support for the former interpretation comes from models that suggest residence of lower crustal melts at low melt fractions (average $F < 0.2$) [*Dufek and Bergantz*, 2005; *Karakas and Dufek*, 2015]. Support for the latter interpretation comes from the observation that magma systems like the YTT contain (rare) magmatic inclusions that reveal recharge by dacitic, often zircon-undersaturated, melts. Zircon saturation temperature for the Toba Caldera Complex Haranggoal dacite ($\leq$830°C; Figure 8), for example, is lower than inferred for eruption (847°C) [*Chesner*, 1998]. Furthermore, xenocrysts are absent from the dacite samples, and Sr isotope signatures of dacites and rhyodacites associated with the Toba Caldera Complex are quite radiogenic ($^{87}Sr/^{86}Sr > 0.7133$) [*Chesner*, 1988].

Those zircons that crystallized at least partly before 501 ka could be cognate to the YTT, or could have been derived from MTT-related volcanic roof rocks that foundered into the magma reservoir [*Bindeman and Valley*, 2001] and/or by incorporation of Toba Caldera Complex plutonic materials. The relatively large volume of the OTT ($\sim$1000 km^3) could suggest a high potential to contribute recycled zircon crystals, a prediction that is not corroborated by the relatively limited contribution from zircon antecrysts older than $\geq$800 ka. Some combination of loss of magmatic and thermal mass (including volatiles) as a result of melt extraction and eruption, reorganization of the magma system, and/or replenishment of the shallow reservoir by dacitic magmas could have isolated and/or dissolved residual zircons that might otherwise have been incorporated in the YTT. In contrast, the number of MTT-related zircons in the YTT eruption (potentially upward of 20%) is surprising given the relatively small size of MTT eruption (60 km^3). Most of these crystals exhibit evidence of post-MTT growth, showing that they were part of the YTT system long before eruption, and evidently semi-continuously before and after the MTT eruption in some cases (Figure 5). These observations, along with the possibility that melts residual after the MTT were high-silica rhyolite [*Chesner*, 2012], favors long durations of zircon stability, and the hypothesis that only a portion of the melt reservoir during the MTT-OTT repose interval may have been evacuated from the Toba Caldera Complex reservoir by eruption of the MTT (Figure 9). This leads to the conclusion that, even though it is a relatively "cold and wet" silicic system, the Toba Caldera Complex persisted at super-solidus conditions for hundreds of thousands of years, as postulated elsewhere for ignimbrite-batholith systems [e.g., *de Silva and Gregg*, 2014; *Lipman and Bachmann*, 2015]. Additionally, we find that instead of near-complete evacuation of the shallow chamber [e.g., *Frazer et al*., 2014], large volcanic eruptions like the 60 km^3 MTT can leave behind significant volumes of crystal residues.

The crystallization age distributions within and between zircon crystals provide compelling evidence for at least intermittent crystal growth over several hundred ka (Figures 3, 5, and 6; supporting information Table S7). Crystallization was dominantly at magmatic, not subsolidus, conditions, and not by vapor deposition in vesicles [*Schmitt*, 2006; *Bacon et al*., 2007], judging by the frequent occurrence of growth (fine-scale oscillatory) zoning and the apparent chemical affinity of most zircons to the range of host melts overall. Zircon growth was periodic at the scale of individual zircons and pumices, and likely in the system overall (Figure 6), and could record periods of more rapid zircon growth. Intervening growth could be absent altogether or, if zircon growth was slow, thin and therefore difficult to detect analytically. Zircon growth rates can be enhanced where melts have high degrees of zircon oversaturation, steep Zr gradients, and relatively high temperatures [*Watson*, 1996; *Wotzlaw et al*., 2013]. Zircon "blooms" may therefore occur when growth is triggered by attainment of a critical level of Zr oversaturation, only to stagnate as the Zr gradient in the liquid relaxes. At the eutectoid conditions that apply to the high-silica rhyolites, zircon growth may be rate-limited to buffering Zr concentrations rather than to steadily decreasing Zr as temperatures fall. Growth rates could also have become Zr diffusion-limited and/or stall as melt becomes isolated in pockets by attainment of mushy conditions (Figure 9) [*Watson*, 1996; *Harrison et al*., 2007].

Peaks in crystallization at hundred thousand year intervals, found in multiple pumices, likely represent episodes of widespread magma reservoir reorganization (Figure 9). These could have included coalescence of different magma batches [*Vazquez and Reid*, 2004; *Ellis et al*., 2014] and/or bottom-up differentiation by magma recharge and melting of cumulates [*Mahood*, 1990; *Couch et al*., 2001; *Bachmann and Bergantz*, 2006]. The associated dissolution of more rimward portions of zircon grains could have contributed to large gaps in the crystallization record. Whether crystallization age "hiatuses" represent attainment of

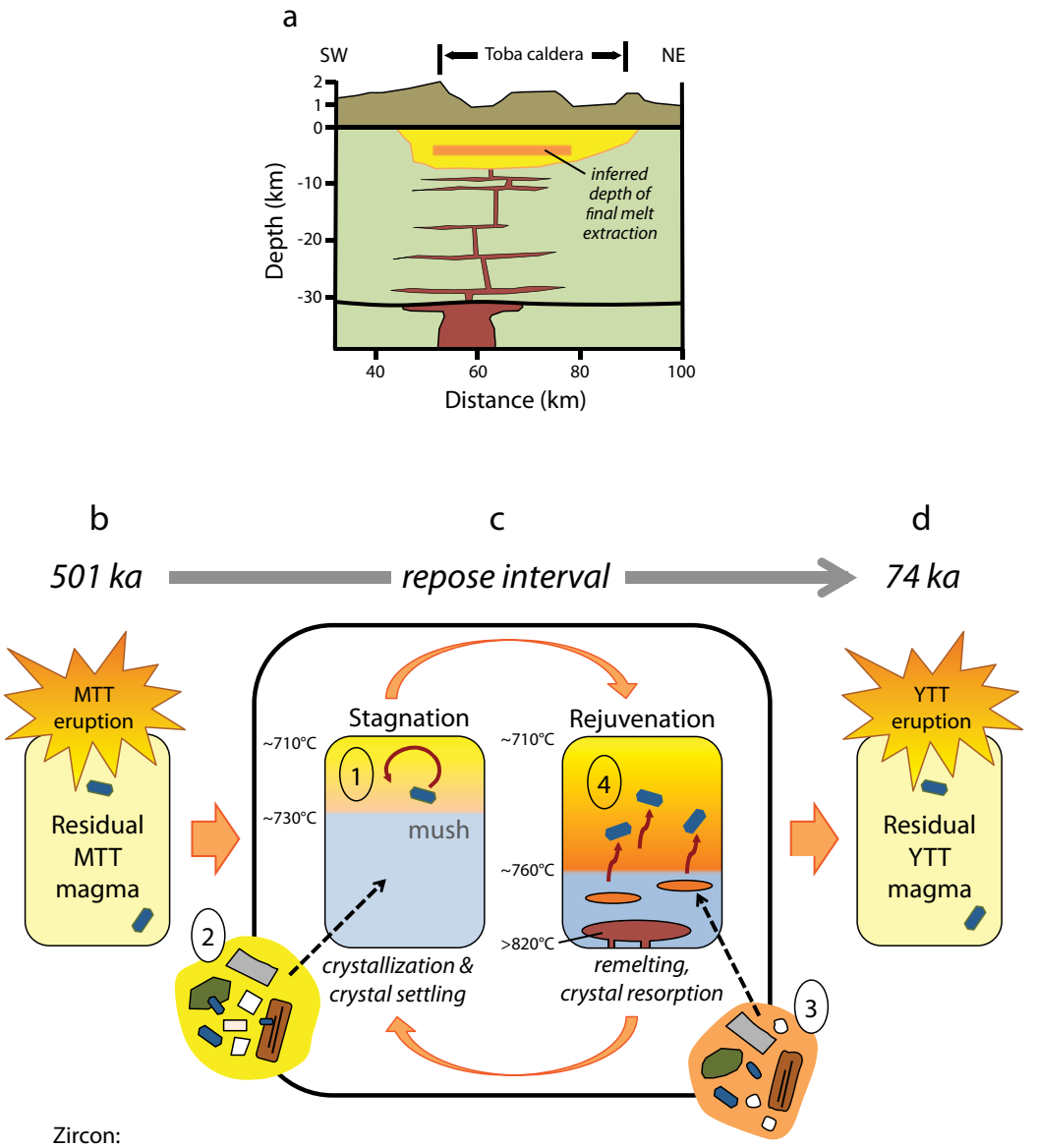

Zircon:

(1) retained in liquid by local scale convection

(2) incorporated in mush as inclusions in major phases or by hindered settling, leading to slowing/ hiatus in growth

(3) released into melt during mush rejuvenation, leading to possible resorption

(4) entrained from mush during melt expulsion

Figure 9. Schematic illustrations of (a) present-day cross section through of the Youngest Toba Tuff (YTT) magma system roughly perpendicular to the long axis of the caldera (Figure 1), and (a–d) evolution of the shallow magma reservoir between eruption of the Middle Toba Tuff (MTT) YTT as inferred from zircon data. Sizes of illustrations are not intended to convey size relations of the magma systems and their components. (a) Sketch of present-day Toba magmatic system based on anisotropy identified by ambient noise seismic tomography and interpretation of crustal velocity (simplified from *Jaxybulatov et al*. [2014]). (b) Magma residual after the MTT eruption becomes part of the YTT magma reservoir. (c) YTT magma reservoir cycles between periods of stagnation and rejuvenation, over which zircon may exist in different environments with associated variations in growth rates, and even partial to complete resorption. Numbered portions of the illustration are linked to enumerated processes. Melt pools in the mush during rejuvenation reflect magma recharge and melts of mush. (d) Magma reservoir evolution interrupted by eruption of the YTT.

eutectoid ± mush-dominated conditions or rejuvenation may be difficult to distinguish because growth may be thin in the former case and absent in the latter, but both processes may occur in tandem before an episode of renewed growth. Zirconium oversaturation would be achieved by cooling following the thermal effects of rejuvenation, compositional changes associated with magma influx (e.g., back-mixing with less

evolved melt) and/or growth of more voluminous melt pools [*Watson*, 1996], in which older zircons already exist or into which they are entrained.

An additional consequence of magma reorganization leading to dissolution of major phases would be release of grains from "zircon nurseries" (Figure 9). Zircon nucleation is favored at grain boundaries of major and accessory phases [*Bacon*, 1989], a condition that may account for the common occurrence of zircon inclusions in YTT biotite, amphibole, and allanite [*Chesner*, 1998]. If remobilized zircon crystals survive resorption, they are unlikely to be subsequently reentrapped in crystals and instead to be mantled by new growth. The same would apply to grains that were never included in other minerals. *Bryan et al*. [2008] estimated that zircon interiors of the size analyzed ($\sim$100 μm) in rhyolites similar in composition and T_{ZS} to the YTT could survive complete resorption at temperatures in excess of saturation for thousands of ka. Small grains, on the other hand, would have been preferentially lost, resulting in the YTT zircon size distributions that have been shown to be deficient in the smallest grain sizes [*Bindeman*, 2003]. Recharge of the system by zircon-saturated melts or high ratios of stored magma to recharge magma would produce less resorption and, possibly, concomitantly less zircon growth. Progressive and preferential growth of melt-hosted zircons is evident from petrographic observation that zircons included in minerals are smaller than those associated with glass.

Resorption and remobilization of crystals in the YTT is evident from minerals besides zircon. As noted above, zoning within some YTT quartz is sharply truncated by rim overgrowths, providing clear evidence for crystal resorption and growth renewal [*Matthews et al*., 2012]. Allanite from the high-silica rhyolite studied here (T54) are both normally and reversely zoned, and crystal growth was likely episodic [*Vazquez and Reid*, 2004]. More radiogenic Ar than expected at eruption dominates the final stages of gases released by step heating of some YTT hornblende and plagioclase [*Gardner et al*., 2002]. As with zircon, early YTT and older crystals of major phases may have been incorporated shortly before to eruption.

7.2. What Insights does Zircon Provide Into the Evolution of Magmatic Zoning?

The compositional heterogeneity of the YTT permits some general predictions about the relative crystallization ages of crystals, against which the dating results for zircons and the compelling evidence for zircon fractionation can be compared. For the end-member case wherein heterogeneity develops by gradual top-down crystal settling [e.g., *Chesner and Luhr*, 2010], compositional evolution would require the low-silica rhyolite crystals to mostly nucleate and grow before the high-silica rhyolite crystals, such that ages would be expected to decrease progressively with increasing whole rock SiO_2. A variant on this differentiation scenario might be a more stepwise process wherein liquids are expressed during mush collapse, such that discrete age differences rather than gradients might be possible. If magma recharge and melting of cumulates contributed to bottom-up differentiation, the picture could be more complicated. Recharge could lead to a net removal of mush crystals by melting, resulting in a large age disparity between accumulated crystals and those of the crystal-poor domain. Alternatively, it could lead to nucleation and growth of younger crystals, including growth on older nuclei that survive resorption. Such scenarios are, of course, simplified for the system of the size of the Toba Tuff, where processes may have been locally heterogeneous and not easily generalized to the system as a whole.

Two first-order observations about the zircon crystallization age distributions that relate to compositional heterogeneity are the following. (1) The U-Pb age rank diagrams in Figure 3 show that the number of MTT aged and older zircon does not differ appreciably with whole rock composition. Notably, the actual proportion of "recycled" grains is greater than the proportion of dates shown because rimming by younger growth results in many of the same grains being also represented in the younger populations. Additionally, at least half of zircon nucleation and growth in all samples occurred in the first half of the MTT-YTT repose interval (mean $^{206}Pb/^{238}U$ dates of 339 $\pm$ 10 ka; mean U-Th core dates of $>$400 ka; Figure 6 and supporting information Table S7). The relatively uniform distribution of older cores and interiors, including recycled grains, represents a crystal background against which later magmatic events occurred. (2) In contrast, the extent of younger zircon growth may depend somewhat on whole rock composition. Zircon spot dates for low-silica rhyolites are dominantly $>$200 ka, whereas dates for zircons from the high-silica rhyolite and the L349D dacite are split approximately equally between this age range and ages younger than 200 ka. This probably cannot be explained by sampling bias, as reference to the zircon depth profiles for high- and low-silica rhyolite shows (Figure 5), as does recognition that the proportion of core analyses is greatest for the dacite. Two

other notable features are that the L349D dacite was apparently able to entrain zircon crystals without dissolving them completely, and the zircons from T54 high-silica rhyolite have the clearest overall trends of decreasing crystallization age and Th/U in core to rim spot analyses (supporting information Table S4). In a compositionally stratified system, these observations could translate to (1) recharge and remobilization in the lowest SiO_2 domains, and (2) gradual growth and attendant cooling of the reservoir's high-silica liquid cap, resulting in quasi-normal trends in crystallization. The more complex depth profiles of grains from the low-silica rhyolite (T57) compared to those of the high-silica rhyolite (T54) could be explained by greater influences from recharge additions and cumulate melting on the former. For the other low-silica rhyolites, if they existed as a distinct domain(s) in the YTT reservoir at this time, they may have been poised at conditions where there was little net growth and possibly even net zircon resorption. Taken together, therefore, the pumice-to-pumice distributions of zircon crystallization age hint at possible partitioning of zircon growth in the final stages of YTT reservoir evolution, possibly because of magmatic stratification.

Independent of the timing of development of compositional heterogeneity, the YTT system apparently underwent repeated recharge and remobilization (Figure 9), as evidenced by a lack in overall secular chemical trend (Figure 7). Zircons were apparently gathered into individual pumices from diverse, albeit typically rhyolitic, domains and Th/U profiles of individual zircons are accordingly complex. Additional evidence for zircon-liquid decoupling is provided by the heterogeneity in oxygen isotope results obtained for zircon grains from a single YTT sample [*Bindeman and Simakin*, 2014]. Zircon rims have $\delta^{18}O$ values within error of expected for equilibrium with the host melt ($\sim$6.7‰). Zircon cores, in contrast, have analytically resolvable heterogeneity in $\delta^{18}O$ ($\sim$6.2–7‰), with values scattering around those of the rims. Consequently, individual zircons can exhibit rimward $\delta^{18}O$ increases or decreases. Diffusional considerations [*Watson and Cherniak*, 1997] show that this heterogeneity can be maintained for a duration of $>$0.5 Ma in zircon crystals the size of the YTT's. In summary, reversals of the chemical and oxygen isotope compositions within zircon crystals lead to a picture of crystals being intermittently entrained by melts into domains where they mix with crystals that have formed in different environments.

7.3. Magma Flux and Evacuation of Giant Cool and Wet Magmas

The longevity of the YTT zircon record is broadly similar to that of one of YTT's closest volumetric peers, the Fish Canyon Tuff [*Bachmann et al*., 2007]. The mean preeruption zircon crystallization age for the 5000 km^3 Fish Canyon Tuff is on the order of $\sim$250 ka [*Wotzlaw et al*., 2013], compared to $\sim$180 ka (U-Th) to $\sim$260 ka (U-Pb) for the 2800 km^3 YTT (supporting information Table S7). Both sets of ages are much greater than mean preeruption age intervals of $<$100 ka compiled by *Simon et al*. [2008] for zircons from the 11 other voluminous silicic explosive eruptions, and could be related to their relatively cool and wet nature [*Lipman and Bachmann*, 2015]. The mean age similarity is especially notable given that, unlike the YTT, the Fish Canyon Tuff is a monotonous crystal-rich dacite. The approximately Gaussian distributions of U-Th and U-Pb zircon spot dates for the YTT, notwithstanding evidence for periodic peaks in crystallization (Figure 6), are also similar to the U-Pb zircon age distributions for the Fish Canyon Tuff. The true distribution of zircon crystallization ages for the YTT is, however, likely skewed somewhat toward the younger side of the age spectrum because spot analyses preferentially sampled interiors, in contrast to analyses of whole zircon crystals for Fish Canyon Tuff. In addition, unlike the FCT, the secular trend in YTT zircon composition is weak, at least to the extent that Th/U can detect it, and does not exhibit a system-wide reversal inferred for the Fish Canyon Tuff to reflect prolonged magma remobilization [*Wotzlaw et al*., 2013].

Caricchi et al. [2014] considered the mode, median, and standard deviation of the Fish Canyon Tuff zircon age population to collectively record a magma flux of $10^{-3}-10^{-2}$ km^3 yr^{-1}. The Caricchi et al. model for characterizing magma fluxes from zircon populations is not strictly applicable to results for the YTT zircons since it assumes that individual zircons crystallize relatively rapidly (1 ka) compared to the overall duration of zircon crystallization; it might nonetheless be broadly generalizable if, as observed for the YTT, volumetrically equivalent growth occurred on many rather than individual grains, and that growth can be quantitatively projected from spot analyzes. As well, the different zircon age distributions for different pumice compositions show that results for samples representing the compositional diversity of the magma reservoir would have to be combined to obtain a complete picture. Nevertheless, minimum intrusion rates would have to have been on the order of 10^{-2} km^3 yr^{-1} if the YTT system grew at steady state in the $\sim$400–500 ka interval spanned by most zircon crystallization ages. Appreciably higher volumes probably pertained because the dominantly high-silica rhyolite of the YTT would have evolved at shallow conditions,

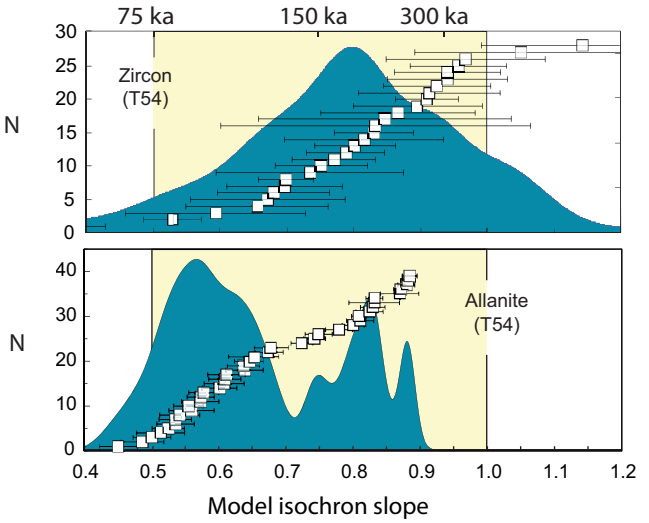

Figure 10. Comparison of probability density populations and rank order plots for spot analyses of zircons (this study) and allanites [*Vazquez and Reid*, 2004] from a high-silica rhyolitic welded tuff (sample T54). Isochron slopes (proportional to crystallization age) are represented to incorporate errors (1σ) symmetrically. Light yellow background delimits the range of isochron slopes from the 74 ka eruption age [e.g., *Storey et al.*, 2012] to secular equilibrium. Note relative youth of allanite compared to zircon and similarity between peaks in allanite isochron slopes to those to those for other zircon populations (Figures 3 and 5).

given the pressure dependence of the ternary eutectoid. Estimated intrusion rates for both the Fish Canyon and Youngest Toba Tuff are similar in magnitude to values of $\geq 10^{-2}$ km^3 yr^{-1} proposed to be required for accumulation of large volumes of silicic magma in the upper crust [*Annen*, 2009].

7.4. Disparate Crystals Records for the YTT Reservoir

There is increasing recognition that time scales obtained from the crystallization ages of major and accessory phases [e.g., *Reid*, 2003; *Cooper and Kent*, 2014; *Chamberlain et al.*, 2014; *Pamukcu et al.*, 2015; *Stelten et al.*, 2015] provide different but complementary perspectives on the durations of magma assembly. Likewise, time scales obtained for YTT quartz and allanite crystallization and storage differ from those for YTT zircon. Quartz interiors are likely at least a few ka old, given that they host faceted melt inclusions [*Chesner and Luhr*, 2010; *Gualda et al.*, 2012b], but final rim growth on quartz may have occurred within only a few ka of eruption at most, based on the lack of Ti diffusional relaxation at the interior boundaries of some quartz rims [*Matthews et al.*, 2012]. Allanite grew nearly continuously in the ~40 ka interval before eruption based on U-Th disequilibria (Figure 10), suggesting that crystals were derived from a magma body that persisted semicontinuously over that time [*Vazquez and Reid*, 2004]. Most zircon interiors for the same sample range to dates much older than those of allanite, even though the pronounced ^{230}Th-^{238}U fractionation by allanite should enable ages of up to ~500 ka to be resolved.

We caution that it is premature to rigorously interpret the apparent differences in zircon, allanite, and quartz age information. Sample T54 represents a welded tuff; younger allanites and zircons could have been derived from pumice, whereas the older zircons could have been winnowed into the ash-rich matrix from other sources. Results for the allanite and quartz also may not be directly comparable because they were performed on compositionally different samples: allanite was hosted in high-silica rhyolite whereas quartz was hosted in low-silica rhyolite. Normal zoning characterizes near-rim quartz domains in the former [*Chesner and Luhr*, 2010] but the latter have subequal proportions of near-rim normal and reversed zoning, at least as imaged [*Matthews et al.*, 2011]. In addition, the timing of quartz growth applies only to the rims whereas that for allanite is across the crystal.

If the temporal records prove to be representative, the following considerations will be important:

1. Zircon is stable across diverse YTT magmatic conditions whereas quartz crystallizes only from high-silica rhyolite; allanite crystallization overlaps that of zircon at low temperature (<~760°C) [*Vazquez and Reid*, 2004]. Accordingly, except in the unlikely case that resorption is rate limiting, zircons will preferentially survive thermal rejuvenation of the YTT chamber compared to allanite and quartz. Secular differences in zircon, allanite and quartz crystallization therefore suggest that, in contrast to long-lived zircon stability, the YTT system only attained sufficient thermal mass and chemical buffering for allanite and quartz persistence ~40 ka and at least a few ka before eruption, respectively. It is nevertheless notable that there are peaks in allanite crystallization ages that are generally concordant with peaks in zircon crystallization ages in the YTT system (e.g., at ~125, ~180, and ~260 ka).
2. Differences in the crystallization ages between the three phases could also be influenced by mechanical separation. Relative to zircon, YTT allanite is expected to settle into the solid-rich cumulate domain

during two-phase flow-related magmatic processes because of its relatively large size (up to 0.6 mm) and density (3.75 kg/m^3). Quartz is less dense but grains up to an order of magnitude smaller than the YTT maximum (~2 cm) could be preferentially settled and locked up in the solid framework of the cumulate domain.

3. Even when growth of all three minerals is favored, growth rates will differ. As noted above, at the eutectoid conditions that apply to the high-silica rhyolites, zircon growth may have served principally to buffer Zr concentrations. Rims of the observed quartz thicknesses (<0.03 cm) could grow in <1000 years [*Gualda et al*., 2012a]; comparably aged zircons might be ≪1 μm thick. Even in the 40 ka of appreciable allanite growth, similarly aged zircon rim growth might still be too thin for existing methods to detect an age progression within them.

8. Summary and Speculative Model for Evolution of the YTT Giant Magma Body

The insights provided by the crystallization record of the giant YTT magma body lead us to propose the following conceptual framework for its evolution (Figure 9). In the aftermath of the ~840 ka eruption of the Oldest Toba Tuff, the Toba Caldera Complex magma reservoir was intermittently rejuvenated by dacitic parent melts that had hybridized significantly with crust at depth. The onset of zircon nucleation occurred at T > 800°C, as melts evolved to low-silica rhyolite. Some fractionation of zircons likely occurred by entrainment as inclusions in crystals and/or in crystal clots. The stochastic nature of this fractionation reflects zircon's affinity for the liquid phase such that, subordinate differences aside, final zircon distributions and mean crystallization ages overlap considerably between pumices.

The YTT magma reservoir was intermittently rejuvenated, resulting in blooms of zircon nucleation and growth in discrete magmatic domains [*Watson*, 1996; *Vazquez and Reid*, 2004]. Mobilization of zircon grains during magma recharge was, like fractionation, stochastic, permitting preferential growth on diverse entrained grains. Individual crystals grew fitfully over hundreds of thousands of years. More subdued peaks in crystal growth could reflect times when the crystal mush was locally rejuvenated by melt perfusion along grain boundaries without appreciable overturn. Major episodes of mush failure/remobilization associated with magma influx was likely responsible for merging of compositional domains and decoupling of zircons and liquids from each other. These events could have lasted for tens of ka by local thermomechanical reactivation involving underplating of dacitic magmas and gas-driven defrosting [*Mahood*, 1990; *Bachmann and Bergantz*, 2006; *Huber et al*., 2011], or even a few hundred years if accompanied by buoyancy-drive overturn ("unzipping") [*Burgisser and Bergantz*, 2011]. Remarkably, major, post-500 ka disruptions to the magma reservoir did not lead to a supereruption.

Significant magmatic influxes into the YTT reservoir in the first half of the MTT-YTT repose interval and development of high-silica rhyolite are recorded by compositionally diverse zircon growth (Figure 7). A magma reservoir that grows by steady state magma (and heat) influx decreases in temperature over time [*Caricchi et al*., 2014], a trend that would enhance the overall probability that once a magma reservoir is zircon-saturated, it will remain so. The reservoir evidently remained poised at conditions between zircon saturation and eutectoid conditions thereafter (Figure 8). In the final ~40 ka before eruption, reservoir conditions were sufficiently cool (±wet?) for allanite to persist in its stability, and regular influxes of melt and growth of the YTT reservoir led to growth of zircons and allanites [*Vazquez and Reid*, 2004; this study]. At these eutectoid conditions, applicable to >50% of the YTT, heat fluxes could dissolve major phases with only a minor effect on larger zircon grains, and zircon growth may have become less synchronized in the YTT reservoir (supporting information Table S7). Chemically distinct melt domains eventually developed, resulting in compositionally affinity between some zircon rims and their host glasses. Mobilization may have been triggered within a few hundred to a few thousand years of eruption, based on the rim reversals on (some) quartz [*Matthews et al*., 2011]. Some crystal cargo was incorporated from a liquid-poor/-absent environment too quickly for growth of "young" rims on some zircons and allanites, and for Ar isotope reequilibration by some plagioclase and hornblende. Eruption may have been triggered by a final propagation of the remobilization front without extensive mixing, related to a major intrusion event, wall rock failure, and/or a pressure release associated with a major earthquake on the Sumatran Fault [*Allan et al*., 2012].

Acknowledgments
We thank Mary Caress, Craig Chesner, Chris Coath, Marty Grove, and Axel Schmitt for their efforts on behalf of this project. We are grateful to Olivier Bachmann, Ben Ellis, Jonathan Miller, and Heather Wright for insightful scientific comments and editorial suggestions that helped to improve this paper. The National Science Foundation, whose grants EAR-9706519, EAR-0003601, and EAR-1322077 enabled us to undertake this research, is gratefully acknowledged. The hospitality and support from ETH Zürich and the University of Washington Helen R. Whiteley Center enabled MR to complete this paper. The ion microprobe facility at the University of California, Los Angeles, is partly supported by a grant from the Instrumentation and Facilities Program, Division of Earth Sciences, National Science Foundation. Any use of trade, firm, or product names is for descriptive purposes only and does not imply endorsement by the U.S. Government. The data used are listed in the supporting information and the references.

References

Aldiss, D. T., and S. A. Ghazali (1984), The regional geology and evolution of the Toba volcano-tectonic depression, Indonesia, *J. Geol. Soc.*, *141*, 487–500.

Allan, A. S. R., C. J. N. Wilson, M.-A. Millet, and R. J. Wysoczanski (2012), The invisible hand: Tectonic triggering and modulation of a rhyolitic supereruption, *Geology*, *40*, 563–566.

Andersen, D. J., and D. H. Lindsley (1988), Internally consistent solution models for Fe-Mg-Mn-ti oxides: Fe-Ti oxides, *Am. Mineral.*, *73*, 714–726.

Annen, C. (2009), From plutons to magma chambers: Thermal constraints on the accumulation of eruptible silicic magma in the upper crust, *Earth Planet. Sci. Lett.*, *284*, 409–416.

Bachmann, O., and G. W. Bergantz (2004), On the origin of crystal-poor rhyolites: Extracted from batholithic crystal mushes, *J. Petrol.*, *45(8)*, 1565–1582.

Bachmann, O., and G. W. Bergantz (2006), Gas percolation in upper-crustal magma bodies as a mechanism for upward heat advection and rejuvenation of silicic crystal mushes, *J. Volcanol. Geotherm. Res.*, *149*, 85–102.

Bachmann, O., F. Oberli, M. A. Dungan, M. Meier, R. Mundil, and H. Fischer (2007), $^{40}Ar/^{39}Ar$ and U–Pb dating of the Fish Canyon magmatic system, San Juan Volcanic field, Colorado: Evidence for an extended crystallization history, *Chem. Geol.*, *236*(1), 134–166.

Bacon, C. R. (1989), Crystallization of accessory phases in magmas by local saturation adjacent to phenocrysts. *Geochim. Cosmochim. Acta*, *53*, 1055–1066.

Bacon, C. R., T. W. Sisson, and F. K. Mazdab (2007), Young cumulate complex beneath Veniaminof caldera, Aleutian arc, dated by zircon in erupted plutonic blocks, *Geology*, *35*, 491–494.

Belousova, E. A., W. L. Griffin, S. Y. O'Reilly, and N. I. Fisher (2002), Igneous zircon: Trace element composition as an indicator of source rock type, *Contrib. Mineral. Petrol.*, *143*, 602–622.

Bindeman, I. N. (2003), Crystal sizes in evolving silicic magma chambers, *Geology*, *31*, 367–370.

Bindeman, I. N., and A. G. Simakin (2014), Rhyolites—Hard to produce, but easy to recycle and sequester: Integrating microgeochemical observations and numerical models, *Geosphere*, *10*, 930–957.

Bindeman, I. N., and J. W. Valley (2001), Low- $\delta^{18}O$ rhyolites from Yellowstone: Magmatic evolution based on analyses of zircons and individual phenocrysts, *J. Petrol.*, *42*, 1491–1517.

Blundy, J., and K. Cashman (2001), Ascent-driven crystallisation of dacite magmas at Mount St Helens, 1980–1986, *Contrib. Mineral. Petrol.*, *140*, 631–650.

Blundy, J., and B. Wood (2003), Mineral-melt partitioning of uranium, thorium and their daughters, *Rev. Mineral. Geochem.*, *52*, 59–123.

Boehnke, P., E. B. Watson, D. Trail, T. M. Harrison, and A. K. Schmitt (2013), Zircon saturation re-revisited, *Chem. Geol.*, *351*, 324–334.

Bohrson, W. A., and M. R. Reid (1998), Genesis of evolved ocean island magmas by deep- and shallow-level basement recycling, Socorro Island, Mexico: Constraints from Th and other isotope signatures, *J. Petrol.*, *39*, 995–1008.

Bryan, S. E., L. Ferrari, P. W. Reiners, C. M. Allen, C. M. Petrone, A. Ramos Rosique, and I. H. Campbell (2008), New insights into crustal contributions to large volume rhyolite generation at the mid-Tertiary Sierra Madre Occidental Province, Mexico, revealed by U-Pb geochronology, *J. Petrol.*, *49*, 47–77.

Burgisser, A., and G. W. Bergantz (2011), A rapid mechanism to remobilize and homogenize highly crystalline magma bodies, *Nature*, *471*, 212–215, doi:10.1038/nature09799.

Caricchi, L., C. Annen, J. Blundy, G. Simpson, and V. Pinel (2014), Frequency and magnitude of volcanic eruptions controlled by magma injection and buoyancy, *Nat. Geosci.*, *7*, 126–130.

Chamberlain, K. J., D. J. Morgan, and C. J. Wilson (2014), Timescales of mixing and mobilisation in the Bishop Tuff magma body: perspectives from diffusion chronometry, *Contrib. Mineral. Petrol.*, *168*, 1–24.

Chesner, C. A. (1988), The Toba Tuff and Caldera Complex, Sumatra, Indonesia: Insights into Magma Bodies and Eruptions. PhD thesis, p. 428, Michigan Technol. Univ., Houghton.

Chesner, C. A. (1998), Petrogenesis of the Toba Tuffs, Sumatra, Indonesia. *J. Petrol.*, *39*, 397–438.

Chesner, C. A. (2012), The Toba Caldera Complex, *Quat. Int.*, *258*, 5–18, doi:10.1016/j.quaint.2011.09.025

Chesner, C. A., and A. D. Ettlinger (1989), Composition of volcanic allanite from the Toba Tuffs, Sumatra, Indonesia, *Am. Mineral.*, *74*, 750–758.

Chesner, C. A., and J. F. Luhr (2010), A melt inclusion study of the Toba Tuffs, Sumatra, Indonesia, *J. Volcanol. Geotherm. Res.*, *197*, 259–278.

Chesner, C. A., W. I. Rose, A. Deino, and R. Drake (1991), Eruptive history of Earth's largest Quaternary caldera (Toba, Indonesia) clarified, *Geology*, *19*, 200–203.

Claiborne, L. L., C. F. Miller, B. A. Walker, J. L. Wooden, F. K. Mazdab, and F. Bea (2006), Tracking magmatic processes through Zr/Hf ratios in rocks and Hf and Ti zoning in zircons: An example from the Spirit Mountain batholith, Nevada, *Min. Mag.*, *70*, 517–543.

Claiborne, L. L., C. F. Miller, D. M. Flanagan, M. A. Clynne, and J. L. Wooden (2010), Zircon reveals protracted magma storage and recycling beneath Mount St. Helens, *Geology*, *38*, 1011–1014.

Cooper, K. M. (2015), Timescales of crustal magma reservoir processes: Insights from U-series crystal ages, *Geol. Soc. Spec. Publ.*, *422*, 141–174.

Cooper, K. M., and A. J. R. Kent (2014), Rapid remobilization of magmatic crystals kept in cold storage, *Nature*, *506*, 480–483.

Couch, S., R. S. J. Sparks, and M. R. Carroll (2001), Mineral disequilibrium in lavas explained by convective self-mixing in open magma chambers, *Nature*, *411*(6841), 1037–1039.

de Silva, S., and P. M., Gregg (2014), Thermomechanical feedbacks in magmatic systems: Implications for growth, longevity, and evolution of large caldera-forming magma reservoirs and their supereruptions, *J. Volcanol. Geotherm. Res.*, *282*, 77–91, doi:10.1016/j.jvolgeores.2014.06.001.

Deering, C. D., and O. Bachmann (2010), Trace element indicators of crystal accumulation in silicic igneous rocks, *Earth Planet. Sci. Lett.*, *297*, 324–331.

Diehl, J. F., T. C. Onstott, C. A. Chesner, and M. D. Knight (1987), No short reversals of Brunhes age recorded in the Toba tuffs, north Sumatra, Indonesia, *Geophys. Res. Lett.*, *14*, 753-756.

Dodson, M. H., W. Compston, I. S. Williams, and J. F. Wilson (1988), A search for ancient detrital zircons in Zimbabwean sediments, *J. Geol. Soc.*, *145*, 977–983.

Dufek, J., and G. W. Bergantz (2005), Lower crustal magma genesis and preservation: A stochastic framework for the evaluation of basalt–crust interaction, *J. Petrol.*, *46*(11), 2167–2195.

Ellis, B. S., O. Bachmann, and J. A. Wolff (2014), Cumulate fragments in silicic ignimbrites: The case of the Snake River Plain, *Geology*, *42*(5), 431–434.
Frazer, R. E., D. S. Coleman, and R. Mills (2014), Zircon U-Pb geochronology of the Mount Givens Granodiorite, central Sierra Nevada, California: Implications for the genesis of large volumes of eruptible magma, *J. Geophys. Res. Solid Earth*, *119*, 2907–2924, doi:10.1002/2013JB010716.
Gardner, J. E., P. W. Layer, and M. J. Rutherford (2002), Phenocrysts versus xenocrysts in the youngest Toba Tuff: Implications for the petrogenesis of 2,800 km^3 of magma, *Geology*, *30*, 347–350.
Gardner, J. E., K. S. Befus, G. A. Gualda, and M. S. Ghiorso (2014), Experimental constraints on rhyolite-MELTS and the Late Bishop Tuff magma body, *Contrib. Mineral. Petrol.*, *168*, 1–14.
Gatti, E., I. M. Villa, H. Achyuthan, P. L. Gibbard, and C. Oppenheimer (2014), Geochemical variability in distal and proximal glass from the Youngest Toba Tuff eruption, *Bull. Volcanol.*, *76*, 859–877.
Gelman, S. E., F. J. Gutiérrez, and O. Bachmann (2013), On the longevity of large upper crustal silicic magma reservoirs, *Geology*, *41*, 759–762.
Ghiorso, M. S., and B. W. Evans (2008), Thermodynamics of rhombohedral oxide solid solutions and a revision of the Fe-Ti- two-oxide geothermometer and oxygen-barometer, *Am. J. Sci.*, *308*, 957–1039, doi:10.2475/09.2008.01.
Grove, M., and T. M. Harrison (1999), Monazite Th–Pb age depth profiling, *Geology*, *27*, 487–490.
Gualda, G. A., and M. S. Ghiorso (2013), Low-pressure origin of high-silica rhyolites and granites, *J. Geol.*, *121*(5), 537–545.
Gualda, G. A., and M. S. Ghiorso (2014), Phase-equilibrium geobarometers for silicic rocks based on rhyolite-MELTS. Part 1: Principles, procedures, and evaluation of the method, *Contrib. Mineral. Petrol.*, *168*(1), 1–17.
Gualda, G. A. R., M. S. Ghiorso, R. V. Lemons, and T. L. Carley (2012a), Rhyolite-MELTS: A modified calibration of MELTS optimized for silica-rich, fluid-bearing magmatic systems, *J. Petrol.*, *53*, 875–890.
Gualda, G. A. R., A. S. Pamukcu, M. S. Ghiorso, A. T. Anderson Jr., and S. R. Sutton (2012b), Timescales of quartz crystallization and the longevity of the Bishop giant magma body, *PLoS ONE*, *7*(5), e37492, doi:10.1371/journal.pone.0037492.
Harrison, T. M., E. B. Watson, and A. B. Aikman (2007), Temperature spectra of zircon crystallization in plutonic rocks, *Geology*, *35*, 635–638.
Hermann, J. (2002), Allanite: thorium and light rare earth element carrier in subducted crust, *Chem. Geol.*, *192*, 289–306.
Huang, R., and A. Audétat (2012), The titanium-in-quartz (TitaniQ) thermobarometer: a critical examination and re-calibration, *Geochim. Cosmochim. Acta*, *84*, 75–89.
Huber, C., O. Bachmann, and J. Dufek (2011), Thermo-mechanical reactivation of locked crystal mushes: Melting-induced internal fracturing and assimilation processes in magmas, *Earth Planet. Sci. Lett.*, *304*, 443–454.
Jaxybulatov, K., N. M. Shapiro, I. Koulakov, A. Mordret, M. Landès, and C. Sens-Schönfelder (2014), A large magmatic sill complex beneath the Toba caldera, *Science*, *346*(6209), 617–619.
Johnson, D. M., P. R. Hooper, and R. M. Conrey (1999), GeoAnalytical Lab, Washington State University, *Adv. X-ray Anal.*, *41*, 843–867.
Karakas, O., and J. Dufek (2015), Melt evolution and residence in extending crust: Thermal modeling of the crust and crustal magmas, *Earth Planet. Sci. Lett.*, *425*, 131–144.
Karlstrom, L., M. L. Rudolph, and M. Manga (2012), Caldera size modulated by the yield stress within a crystal-rich magma reservoir, *Nat. Geosci.*, *5*, 402–405, doi:10.1038/NGEO1453.
Knight, M. D., G. L. Walker, B. B. Ellwood, and J. F. Diehl (1986), Stratigraphy, paleomagnetism, and magnetic fabric of the Toba tuffs: constraints on the sources and eruptive styles, *J. Geophys. Res.*, *91*, 355-382.
Kularatne, K., and A. Audétat (2014), Rutile solubility in hydrous rhyolite melts at 750–900° C and 2kbar, with application to titanium-in-quartz (TitaniQ) thermobarometry, *Geochim. Cosmochim. Acta*, *125*, 196–209.
Lipman, P. W., and O. Bachmann (2015), Ignimbrites to batholiths: Integrating perspectives from geological, geophysical, and geochronological data, *Geosphere*, *11*(3), 705–743.
Loewen, M. W., and I. N. Bindeman (2016), Oxygen isotope thermometry reveals high magmatic temperatures and short residence times in Yellowstone and other hot-dry rhyolites compared to cold-wet systems, *Am. Mineral.*, *101*(5), 1222–1227.
Ludwig, K. A. (2003), *Isoplot/Ex ver. 3.00, A Geochronological Tool Kit for Microsoft Excel, Spec. Publ. 4*, Berkeley Geochronol. Cent., Berkeley, Calif.
Lundstrom, C. C., and A. F. Glazner (2016), Silicic magmatism and the volcanic-plutonic connection, *Elements*, *12*(2), 91–96.
Mahood, G. A. (1990), Second reply to comment of R.S.J. Sparks, H.E. Huppert and C.J.N. Wilson on "Evidence for long residence times of rhyolitic magma in the Long Valley magmatic system: The isotopic record in the precaldera lavas of Glass Mountain", *Earth Planet. Sci. Lett.*, *99*, 395–399.
Mark, D. F., M. Petraglia, V. C. Smith, L. E. Morgan, D. N. Barfod, B. S. Ellis, N. J. Pearce, J. N. Pal, and R. A. Korisettar (2013), A high-precision $^{40}Ar/^{39}Ar$ age for the Young Toba Tuff and dating of ultra-distal tephra: Forcing of Quaternary climate and implications for hominin occupation of India, *Quat. Geochron.*, *21*, 90–103.
Matthews, N. E., C. Huber, D. M. Pyle, and V. C. Smith (2012), Timescales of magma recharge and reactivation of large silicic systems from Ti diffusion in quartz, *J. Petrol.*, *53*, 1385–1416.
Miller, C. F., S. M. McDowell, and R. W. Mapes (2003), Hot and cold granites? Implications of zircon saturation temperatures and preservation of inheritance, *Geology*, *31*, 529–532.
Mojzsis, S. J., and T. M. Harrison (2002), Establishment of a 3.83 Ga magmatic age for the Akilia tonalite (southern West Greenland), *Earth Planet. Sci. Lett.*, *202*, 563–576.
Ninkovich, D., N. J. Shackleton, A. A. Abdel-Monem, J. D. Obradovich, and G. Izett (1978), K-Ar age of the late Pleistocene eruption of Toba, north Sumatra, *Nature*, *276*, 574–577.
Nishimura, S., E. Abe, T. Yokoyama, S. Wirasantosa, and A. Dharma (1977), Danau Toba—The outline of Lake Toba, North Sumatra, Indonesia, *Paleolimnol. Lake Biwa Jpn. Pleistocene*, *5*, 313-332.
Pamukcu, A. S., G. A. Gualda, F. Bégué, and D. M. Gravley (2015), Melt inclusion shapes: Timekeepers of short-lived giant magma bodies, *Geology*, *43*(11), 947–950.
Paterson, S. R., and M. N. Ducea (2015), Arc magmatic tempos: Gathering the evidence, *Elements*, *11*(2), 91–98.
Petraglia, M. D., R. Korisettar, and J. N. Pal (2012), The Toba volcanic super-eruption of 74,000 years ago: Climate change, environments, and evolving humans, *Quat. Int.*, *258*, 1–4.
Reid, M. R. (2003), Timescales of magma transfer and storage in the crust, in *The Crust. Treatise on Geochemistry*, vol. 3, edited by R. L. Rudnick, pp. 167–193, Elsevier, Oxford, U. K.
Reid, M. R., and C. D. Coath (2000), In situ U–Pb ages of zircons from the Bishop Tuff: No evidence for long crystal residence times, *Geology*, *28*(5), 443–446.

Reid, M. R., C. D. Coath, T. M. Harrison, and K. D. McKeegan (1997), Prolonged residence times for the youngest rhyolites associated with Long Valley Caldera: Th-230-U-238 ion microprobe dating of young zircons, *Earth Planet. Sci. Lett.*, *150*(1–2), 27–39.

Reid, M. R., J. A. Vazquez, and A. K. Schmitt (2011), Zircon-scale insights into the history of a supervolcano, Bishop Tuff, Long Valley, California—With implications for the Ti-in-zircon geothermometer, *Contrib. Mineral. Petrol.*, *161*, 313–331.

Sambridge, M. S., and W. Compston (1994), Mixture modeling of multicomponent data sets with application to ion-probe zircon ages, *Earth Planet. Sci. Lett.*, *128*(3–4), 373–390.

Schmitt, A. K. (2006), Laacher See revisited: High-spatial-resolution zircon dating indicates rapid formation of a zoned magma chamber, *Geology*, *34*, 597–600.

Schmitt, A. K., M. Grove, T. M. Harrison, O. Lovera, J. Hulen, and M. Walters (2003), The Geysers—Cobb Mountain Magma System, California (Part 1): U-Pb zircon ages of volcanic rocks, conditions of zircon crystallization and magma residence times, *Geochim. Cosmochim. Acta*, *67*(18), 3423–3442.

Schmitt, A. K., D. F. Stockli, S. Niedermann, O. M. Lovera, and B. P. Hausback (2010), Eruption ages of Las Tres Virgenes volcano (Baja California): A tale of two helium isotopes, *Quat. Geochron.*, *5*(5), 503–511.

Self, S. (2006), The effects and consequences of very large explosive volcanic eruptions, *Philos. Trans. R. Soc. A*, *364*, 2073–2097.

Simon, J. I., P. R. Renne, and R. Mundil (2008), Implications of pre-eruptive magmatic histories of zircons for U–Pb geochronology of silicic extrusions, *Earth Planet. Sci. Lett.*, *266*(1–2), 182–194.

Stelten, M. E., K. M. Cooper, J. A. Vazquez, A. T. Calvert, and J. J. Glessner (2015), Mechanisms and timescales of generating eruptible rhyolitic magmas at Yellowstone caldera from zircon and sanidine geochronology and geochemistry, *J. Petrol.*, *56*, 1607–1642.

Storey, M., R. G. Roberts, and M. Saidin (2012), Astronomically calibrated $^{40}Ar/^{39}Ar$ age for the Toba supereruption and global synchronization of late Quaternary records, *Proc. Natl. Acad. Sci. U. S. A.*, *109*, 18,684–18,688.

Storm, S., P. Shane, A. K. Schmitt, and J. M. Lindsay (2012), Decoupled crystallization and eruption histories of the rhyolite magmatic system at Tarawera volcano revealed by zircon ages and growth rates, *Contrib. Mineral. Petrol.*, *163*, 505–519.

Thomas, J. B., E. B. Watson, F. S. Spear, P. T. Shemella, S. K. Nayak, and A. Lanzirotti (2010), TitaniQ under pressure: The effect of pressure and temperature on the solubility of Ti in quartz, *Contrib. Mineral. Petrol.*, *160*, 743–759.

Thomas, J. B., E. B. Watson, F. S. Spear, and D. A. Wark (2015), TitaniQ recrystallized: experimental confirmation of the original Ti-in-quartz calibrations. *Contrib. Mineral. Petrol.*, *169*, 1–16.

Trail, D., S. J. Mojzsis, and T. M. Harrison,(2007), Thermal events documented in Hadean zircons by ion microprobe depth profiles, *Geochim. Cosmochim. Acta*, *71*, 4044–4065.

Turner, S. P., and J. D. Foden (2001), U-Th-Ra disequilibria, Sr-Nd-Pb isotope and trace element variations in Sunda arc lavas: Predominance of a subducted sediment component, *Contrib. Mineral. Petrol.*, *142*, 43–57.

Vazquez, J. A., and M. R. Reid (2004), Probing the accumulation history of the voluminous Toba magma, *Science*, *305*(5686), 991–994.

Wark, D. A., and E. B. Watson (2006), TitaniQ: A titanium-in-quartz geothermometer, *Geochim. Cosmochim. Acta*, *152*, 743–754.

Wark, D. A., W. Hildreth, F. S. Spear, D. J. Cherniak, and E. B. Watson (2007), Pre-eruption recharge of the Bishop magma system, *Geology*, *35*(3), 235–238.

Watson, E. B. (1996), Dissolution, growth and survival of zircons during crustal fusion: Kinetic principles, geological models and implications for isotopic inheritance, *GSA Spec. Pap.*, *315*, 43–56.

Watson, E. B., and D. J. Cherniak (1997), Oxygen diffusion in zircon, *Earth Planet. Sci. Lett.*, *148*(3), 527–544.

Watson, E. B., and T. M. Harrison (1983), Zircon saturation revisited—Temperature and composition effects in a variety of crustal magma types, *Earth Planet. Sci. Lett.*, *64*, 295–304.

Westgate, J. A., N. J. G. Pearce, W. T. Perkins, S. J. Preece, C. A. Chesner, and R. F. Muhammad (2013), Tephrochronology of the Toba tuffs: Four primary glass populations define the 75-ka Youngest Toba Tuff, northern Sumatra, Indonesia, *J. Quat. Sci.*, *28*, 772–776.

White, S. M., J. A. Crisp, and F. J. Spera (2006), Long-term volumetric eruption rates and magma budgets, *Geochem. Geophys., Geosyst.*, *7*, Q03010, doi:10.1029/2005GC001002.

Wolff, J. A., B. S. Ellis, F. C. Ramos, W. A. Starkel, S. Boroughs, P. H. Olin, and O. Bachmann (2015), Remelting of cumulates as a process for producing chemical zoning in silicic tuffs: A comparison of cool, wet and hot, dry rhyolitic magma systems, *Lithos*, *236*, 275–286.

Wotzlaw, J.-F., U. Schaltegger, D. A. Frick, M. A. Dungan, A. Gerdes, and D. Günther (2013), Tracking the evolution of large-volume silicic magma reservoirs from assembly to supereruption, *Geology*, *41*, 867–870.

Yokoyama, T., and P. E. Hehanussa (1981), The age of "Old Toba Tuff" and some problems on the geohistory of Lake Toba, Sumatra, Indonesia, in *Paleolimnology of Lake Biwa and the Japanese Pleistocene*, vol. 9, edited by S. Horie, pp. 177–186, Kyoto University, Kyoto, Japan.